An epitope-resurfaced virus-like particle can induce broad neutralizing antibody against four serotypes of dengue virus

Authors: Wen-Fan Shen[1][§], Jedhan Ucat Galula[2][§], Jyung-Hurng Liu[3][§], Mei-Ying Liao[2][§], Chang-Hao Huang[2], Yu-Chun Wang[2], Han-Chung Wu[4], Jian-Jong Liang[5], Yi-Ling Lin[5], Matthew T. Whitney[6], Gwong-Jen J. Chang[6], Sheng-Ren Chen[8], Shang-Rung Wu[7,8][*] Day-Yu Chao[2][§]*

Affiliations:

[1] Ph.D. Program in Microbial Genomics, National Chung-Hsing University, Taichung, Taiwan.

[2] Graduate Institute of Microbiology and Public Health, College of Veterinary Medicine, National Chung-Hsing University, Taichung, Taiwan.

[3] Institute of Genomics and Bioinformatics, College of Life Science, National Chung-Hsing University, Taichung, Taiwan.

[4] Institute of Cellular and Organismic Biology, Academia Sinica, Taipei, Taiwan

[5] Institute of Biomedical Sciences, Academia Sinica, Taipei, Taiwan

[6] Division of Vector-Borne Diseases, Centers for Disease Control and Prevention, Fort Collins, Colorado, USA.

[7] Institute of Basic Medical Sciences, College of Medicine, National Cheng Kung University, Tainan, Taiwan

[8] Institute of Oral Medicine, College of Medicine, National Cheng Kung University, Tainan, Taiwan

§These authors contributed equally to this work

Word counts: 287 words (Abstract),   7595 words (main text)

Running title: Epitope-resurfaced dengue VLP

[*] **Corresponding authors**

Day-Yu Chao, Ph.D.

32   Graduate Institute of Microbiology and Public Health, College of Veterinary Medicine

33   National Chung-Hsing University

34   Taichung 402, Taiwan

35   TEL:886-4-22840694

36   FAX:886-4-22852186

37   EMAIL: dychao@nchu.edu.tw

38   Or

39   Shang-Rung Wu**,** Ph.D.

40   Institute of Oral Medicine, College of Medicine,

41   National Cheng Kung University,

42   Tainan 701, Taiwan

43   TEL:886-6-2353535

44   FAX:886-6-2359885

45   EMAIL: z10208056@email.ncku.edu.tw

46   **Abstract**

47   Dengue fever is caused by four different serotypes of dengue virus (DENV) which is the leading

48   cause of worldwide arboviral diseases in humans. Virus-like particles (VLPs) containing

49   flavivirus prM/E proteins have been demonstrated to be a potential vaccine candidate; however,

50   the structure of dengue VLP is poorly understood. Herein we show for the first time that

51   mD2VLP particles possess a T=1 icosahedral symmetry with a groove located within the E-

52   protein dimers near the 2-fold vertices that exposed highly overlapping, cryptic neutralizing

53   epitopes through cryo-electron microscopy reconstruction. Mice vaccinated with highly matured

54   virus-like particles derived from DENV serotype 2 (mD2VLP) can generate higher cross-

55   reactive (CR) neutralization antibodies (NtAbs) and were protected against all 4 serotypes of

56   DENV through clonal expansion supported by hybridoma and B-cell repertoire analysis. Our

57   results revealed that a "epitope-resurfaced" mature-form dengue VLP has the potential to induce

58   quaternary structure-recognizing broad CR NtAbs.

59

60

Introduction

Dengue virus (DENV), a member of the family *Flaviviridae*, is a mosquito-borne pathogen with four distinct serotypes, DENV-1 to DENV-4(Lindenbach and Rice). It has been estimated that DENV infects about 390 million individuals globally each year, resulting in 96 million clinically apparent infections ranging from mild fever to the life-threatening dengue hemorrhagic fever (DHF) or dengue shock syndrome (DSS)(Bhatt et al., 2013). Although the chimeric yellow fever 17D-derived, tetravalent dengue vaccine (CYD-TDV) has recently been approved by the governments of a few DENV-circulating countries, the unexpected low vaccine efficacy in dengue-naïve children or children younger than 6 years old has limited the use of this vaccine in the 9-45 age group living in endemic countries(Guy and Jackson, 2016). Developing a new strategy by either improving the efficacy of CYD-TDV(Aguiar et al., 2016;Halstead, 2017;World Health Organization, 2017) or the second-generation vaccine candidates(Kirkpatrick et al., 2016) is essential to broaden the coverage for all vulnerable populations.

The envelope (E) protein of DENV on the surface of viral particles is the major target of neutralizing antibodies (NtAbs)(Roehrig, 2003;Pierson et al., 2008). The ectodomain of the E protein contains three distinct domains, EDI, EDII, and EDIII, which are connected by flexible hinges to allow rearrangement of domains during virus assembly, maturation and infection(Modis et al., 2003). However, the immune response from humans who have recovered from primary DENV infections is dominated by cross-reactive (CR), non-NtAbs which recognize mainly pre-membrane (prM) or fusion loop of the E (FLE) protein(Dejnirattisai et al., 2010). During virus replication, newly synthesized DENVs are assembled as immature particles

4

83   in the endoplasmic reticulum at neutral pH, followed by translocation through the trans-Golgi

84   network and low-pH secretory vesicles(Chambers et al., 1990). The pr portion of the prM

85   protein, positioned to cover the fusion loop (FL) peptide at the distal end of each E protein,

86   prevents premature fusion during the virion maturation process along the egress pathway from

87   the infected cells(Li et al., 2008;Kostyuchenko et al., 2013). For DENV to become fully

88   infectious, the pr molecule has to be removed by a cellular furin protease during the egress

89   process(Rodenhuis-Zybert et al., 2010). However, furin cleavage in the low-pH secretory

90   vesicles is thought to be inefficient; hence, DENV particles released from infected cells are

91   heterogeneous populations with different degrees of cleavage and release of the pr portion of

92   prM to form the mature membrane (M) protein(Pierson and Diamond, 2012). Immature DENV

93   (imDENV) particles consist of uncleaved prM protein and partially immature particles

94   (piDENV) containing both prM and M proteins, while fully mature DENV (mDENV) contains

95   only M protein(Junjhon et al., 2010;Pierson and Diamond, 2012). Functional analyses have

96   revealed that a completely immature flavivirus lacks the ability to infect cells unless in the

97   presence of anti-prM antibodies through a mechanism called antibody-dependent enhancement

98   (ADE) of infection(Dejnirattisai et al., 2010;Rodenhuis-Zybert et al., 2010;Rodenhuis-Zybert et

99   al., 2011;da Silva Voorham et al., 2012). ADE plays an important role in dengue pathogenesis,

100   and is potentially modulated by the antibody concentration and the degree of virion maturity

101   (Nelson et al., 2008;Rodenhuis-Zybert et al., 2015).

102

103   Virus-like particles (VLPs) containing flavivirus prM/E proteins have been demonstrated

104   to be a potential vaccine candidate, since their ordered E structures are similar to those on the

105   virion surface and also undergo low-pH-induced rearrangements and membrane fusion similar to

106   viral particles(Allison et al., 1995). Also, VLP vaccines present several advantages since they are

107   highly immunogenic, non-infectious, and accessible to quality control as well as increased

108   production capacity. However, we theorized that the process of VLP maturation might be similar

109   to that of dengue viral particles, with heterogeneous pr-containing structures. In this study, we

110   engineered and characterized the structure of mature DENV-2 VLPs through cryo-EM. The

111   immunological properties of mature VLPs were further compared with its immature counterparts.

112

113

114

115   **Results**

116   As we theorized, the process of VLP maturation are similar to that of dengue viral

117   particles so that the wild-type particles (wtD2VLP) produced from the cells are partially

118   immature containing both prM and M proteins (Figure S1 in Supplementary Material). To

119   overcome this problem, we engineered the DENV-2 VLPs as completely mature particles by

120   manipulating the furin cleavage site at the junction of pr and M in a DENV-2 VLP-expressing

121   plasmid(Chang et al., 2003). For comparison, we also generated immature VLP (imD2VLPs) by

122   mutating the minimal furin cleavage motif REKR to REST(Li et al., 2008), which resulted in

123   completely uncleaved prM as detected by western blot and ELISA (Figure 1). Generation of

124   mature DENV-2 VLP (mD2VLP) was much more challenging. First, we performed multiple

125   sequence alignments of the pr/M junction from several flaviviruses, including the distance-

126   related cell fusion agent virus (CFAV), and analyzed their furin cleavage potential using the

127   algorithm PiTou 2.0(Tian et al., 2012). DENV-3 pr/M junction had the lowest predicted Pitou

128   score of 6.87, while WNV had the highest score of 15.4 (Figure 1A). Secondly, we determined

129   the cleavage efficiency of D2VLP by replacing P1-8 at the pr/M junction site of DENV-2 with

130   sequences from different flaviviruses. Although the Pitou prediction of the CFAV pr/M junction

131   did not result in a high score for cleavage, replacement with P1-8 of CFAV resulted in the most

132   efficient furin cleavage for D2VLP, with only 31% of prM remaining uncleaved as compared to

133   the 100% uncleaved imD2VLP (Figure 1A). An additional mutation in the P3 residue from E to

134   S of the CFAV P1-8 construct reduced the prM signaling to 13.7% of that of imD2VLP. We thus

135   named this construct with the replacement of CFAV P1-8 plus the P3 E to S mutation as

136   mD2VLP. The pr/M cleavage of this construct was increased to nearly 90% (Figure 1B). Similar

137   to wtD2VLP purified from plasmids transfected culture supernatants, the mD2VLP and

138   imD2VLP showed consistent conformational integrity as ascertained by similar equilibrium

139   banding profiles in 5-25% sucrose density gradients, as well as comparable particle size

140   distributions as determined by negative staining electron microscopy, and complex glycosylation

141   on the E proteins (Figure S2 in Supplementary Material).

142

143   Previous study has shown molecular organization of recombinant VLPs from tick-borne

144   encephalitis virus (TBEV)(Ferlenghi et al., 2001). However, the cryo-EM results showed low

145   resolution due to particle size heterogeneity and no immunological data can be derived from such

146   structure. To better understand if the structural organization of mD2VLP is similar to that of

147   TBEV and its immunological characteristics, purified mD2VLPs were subjected to cryo-EM

148   analysis. The results demonstrated that the mD2VLPs had a variable size distribution (Figure S3

149   in Supplementary Material). The size variation made improving the resolution challenging,

150   however we were able to determine the overall morphology and E arrangement of mD2VLP

151   based on current achieved resolution. Using a dengue virus-specific Mab (MAb32-6)(Li et al.,

152   2012), immunogold labeling detected the mD2VLPs as spherical particles with a diameter of

153   ~31 nm (Figure S4 in Supplementary Material), which was also the major population as shown

154   in Supplementary Figure S3B. Besides, the particles with diameter of ~31nm had more solid

155   features in 2D image analyses (Figure S3 in Supplementary Material) and were able to obtain

156   stable structure than other groups. Therefore, we continued and focused on this population for

157   further 3D reconstruction and image analyses. The results showed that mD2VLPs with the

158   diameter of ~31nm at a resolution of 13.1Å had a hollow structure and smooth surface with

159   protrusions around the 5-fold positions (Figure 2A, left, and Figure S5 in Supplementary

160   Material). Fitting the atomic E and M surface proteins (PDB: 3J27) into the cryo-EM density

161   map showed that the mD2VLPs have 60 copies of E packed as dimers in a T=1 icosahedral

162   surface lattice (Figure 2A, right). The apparent differences of structural features on the

163   mD2VLPs compared to the mature native virion particles(Kostyuchenko et al., 2013;Zhang et

164   al., 2013a) was a slimmer lipid bilayer and the rearrangements of the surface proteins. First, the

165   central section through the viron and m2DVLP reconstructions showed that the bilayer of

166   m2DVLP was relatively thinner than that of viron. The distance between the exterior leaflet and

167   the interior leaflet of m2DVLP and virion was 12Å and 14Å, respectively (Figure 2B). A similar

168   T=1 icosahedral symmetry of the E-protein arrangement and thinner lipid bilayer were also

169   found in TBEV VLPs(Ferlenghi et al., 2001). Second, interpretation of the map showed that E

170   dimer subunits moved apart from each other causing less density in the intra-dimeric interphase

171   (Figure 3C). Because of this loose interaction, a groove located within the E-protein dimer near

172   the icosahedral 2-fold vertices on mD2VLP was noted (Figure 3A, right, and Figure S6 in

173   Supplementary Material). Third, the central section showed that there was a solid density in the

174   H-layer, which is composed of H helices of E and M protein stem regions, while the density in

175   the T-layer, which contains transmembrane helices of E and M proteins, was weaker in the VLP

176   (Figure 2B). Each E protein consists of an E ecto-domain and a stem region that connects the

177   ecto-domain to its transmembrane region. The stem contains two α-helices, one of which

178   interacts with the viral lipid membrane and the other with the E ecto-domain. This looser

179   interaction of E protein dimers was further stabilized by the E protein rearrangement and the

180   closer interaction with one of the α-helices, which resulted in the solid density beneath the ecto-

9

181   domain as shown in Figure 2B. It is worth noting that the stem region of this mD2VLP was

182   replaced into Japanese Encephalitis viral (JEV) sequence; it was previously suggested that this

183   replacement increased the hydrophobicity for the interaction with the lipid membrane and

184   enhanced the secretion of dengue VLP(Purdy and Chang, 2005).

185

186   Next, we speculated that the structure of mD2VLP with a groove located within the E-

187   protein dimer could affect the epitope presentation on the surface of the particles. First, we

188   calculated the solvent accessibility of mD2VLP and compared the results with that of DENV-2

189   virion. This rearrangement of E protein under T=1 symmetry on the VLP surface exposed more

190   accessible epitopes (48.2%; 191 amino acid with $\geq$30% solvent accessibility among 396 amino

191   acids of the entire E protein) compared to DENV-2 virions (43.4%; 172 amino acid), particularly

192   located at fusion loop, aa 239, aa 251-262 of EDII which together formed the groove, and at A

193   strand, cd loop and G strand of EDIII which surrounded a 5-fold axis (Figure 3A, left, Figure S7

194   in Supplementary Material). Footprint analysis (Figure 3B) showed that those cryptic residues on

195   the E protein, which were previously buried inside of the native DENV virion and only

196   interacted with the broad NtAbs while the virion "breathed"(Lok, 2016), were better exposed on

197   the m2DVLP. Specifically, the epitopes interacting with MAb 1A1D-2, which binds to the virus

198   at 37$^\mathrm{o}$C(Lok et al., 2008); MAb 2D22, which could block two-thirds of all dimers on the virus

199   surface, depending on the strain(Fibriansah et al., 2015a); and the 'E-dimer-dependent epitope',

200   which is recognized by broadly neutralizing MAbs EDE1 and 2(Rouvinski et al., 2015), were all

201   well-exposed in VLPs without steric hindrance. Second, a panel of murine MAb, recognizing

202   different domains of E protein and used previously for antigenic mapping(Crill et al., 2012), was

10

203 subjected to binding-ELISA (Figure S8 in Supplementary Material). The results confirmed that

204 most of the Mabs preferentially binds to mD2VLP, in particularly Mabs recognizing domain I/II

205 (Figure 4).

206

207   To further determine the influence of prM cleavage on the immunogenicity of D2VLP,

208 we immunized groups of 4-week-old BALB/c mice with the purified wtD2VLP, imD2VLP or

209 mD2VLP (4 μg/mouse) twice at a 4-week interval. To better represent the neutralizing

210 antibodies at the late convalescent phase, serum samples collected at 8 weeks after the boost

211 were analyzed by antigen-specific ELISA for antibody response against homologous D2VLP

212 antigens with different maturity profiles. In order to precisely quantify the amount of dengue-

213 specific antibodies, we used the same quantity of purified VLPs in the antigen-capture ELISA

214 (Figure 5A). WtD2VLP and imD2VLP induced similar ELISA titers of DENV-2-specific IgG

215 antibody against three VLP antigens. However, stronger reactivity against the mature antigen

216 was noted with mD2VLP immunization (1:15,347 vs. 1:6,381 vs. 2,529 for mD2VLP, imD2VLP

217 and wtD2VLP, respectively) (Figure 5B). We also analyzed the neutralizing ability of these sera

218 against the four serotypes of DENV using a 50% antigen focus-reduction micro neutralization

219 test (FRμNT$_{50}$). The mD2VLP immunization group induced a higher and broader neutralizing

220 antibody response against all 4 serotypes of DENV (FRμNT$_{50}$ for DENV-1=1:331, DENV-

221 2=1:597, DENV-3=1:70 and DENV-4=1:141), as compared to the imD2VLP vaccinated group

222 (FRμNT$_{50}$ for DENV-1=1:100, DENV-2=1:207 DENV-3=1:64 and DENV-4=1:76) (Figure 5C).

223

11

224   Since the amino acid sequence is identical except for the mutations at the furin cleavage

225   site, the difference in antibody binding and neutralizing activity between mD2VLP and

226   imD2VLP vaccinated mice sera could result from the difference in induction of CR anti-prM

227   non-NtAbs or anti-E NtAbs recognizing structure-dependent epitopes. To address whether the

228   higher neutralization activity induced by mD2VLP was partly due to the reduction of anti-prM

229   antibodies that are known to be cross-reactive but have no neutralizing activity(Dejnirattisai et

230   al., 2010), we performed epitope-blocking ELISAs by using an anti-prM-specific monoclonal

231   antibody (MAb 2H2). MAb 2H2 blocked only 7.59% of the activity of anti-mD2VLP sera but

232   blocked up to 35.26% of antibodies from the imD2VLP-vaccinated groups (Figure S9 in

233   Supplementary Material). To avoid steric hindrance due to Mab 2H2 binding, we performed site-

234   directed mutagenesis on three amino acids of pr protein based on the following criteria: (1) the

235   conservation of amino acids among all four serotypes; (2) residues interacting with MAb

236   2H2(Wang et al., 2013); (3) residues not interfering with prM and E interaction(Li et al., 2008).

237   As shown in supplementary Figure S10, K26P was a key residue, which significantly decreased

238   the binding of both MAb 2H2 and 155-49 (another cross-reactive murine Mab recognizing pr

239   protein(Huang et al., 2006)). However, only the mutant Δ2H2-imD2VLP with F1A, K21D and

240   K26P amino acid triple mutations completely prevent the binding of both MAb 2H2 and 155-49

241   but not that of DENV-2, E-specific Nt-MAb 3H5 (Figure S11 in Supplementary Material). The

242   sera from immunized mice were tested for their binding ability to the wild-type and mutant-

243   Δ2H2 imD2VLP. The differences in binding of imD2VLP and Δ2H2 imD2VLP was greater for

244   the anti-imD2VLP sera than the anti-mD2VLP sera (Figure 5D and E), suggesting that compared

245   to mD2VLP, imD2VLP was more likely to induce 2H2-like anti-prM antibodies. Thus,

246   mD2VLP has the advantage of eliciting lower levels of anti-prM CR antibody and inducing

247   antibodies with greater neutralizing activity.

248

249   The preservation of neutralizing epitopes on the surface of VLPs is critical for efficient

250   production of broadly neutralizing antibody responses. Recent studies have suggested that human

251   monoclonal antibodies (MAbs) reactive with all dengue serotypes can neutralize DENV in the

252   low picomolar range. These MAbs have a preference to bind at the envelope dimer epitopes

253   preserved on virion particles with a high degree of maturity(Dejnirattisai et al., 2015;Rouvinski

254   et al., 2015). We next investigated if a broad neutralization response to mD2VLP immunization

255   was due to the induction of antibodies with a preference to bind at the E dimer epitopes

256   preserved on the surface of mature VLP(Dejnirattisai et al., 2015;Rouvinski et al., 2015). The

257   splenocytes from mD2VLP-vaccinated mice were used to perform fusion and generate

258   hybridomas. Among 2,836 hybridomas screened, two MAbs with high reactivities to VLP

259   measured by ELISA and FRμNT$_{50}$ were shown in Figure 6. As shown in Figure 6A, DM8-6 is a

260   serotype-specific MAb reactive only with DENV-2; while MAb DM25-3 recognized all four

261   serotypes of DENV. Next, we tested the neutralizing activity of these two MAbs against four

262   serotypes of DENV. DM8-6 showed good neutralizing activity against DENV-2 at a

263   concentration of 0.037 μg/mL in FRμNT$_{50}$ but poorly neutralized the other three serotypes.

264   Consistent with the ELISA results, DM25-3 neutralized all four serotypes in FRμNT$_{50}$ at 0.32,

265   0.38, 0.24 and 0.58 μg/mL for DENV-1 to DENV-4, respectively (Figure 6B).

266

267   To determine if MAb DM25-3 recognized quaternary structure-dependent epitopes

268   presented only on mature virion particles(Fibriansah et al., 2015a;Rouvinski et al., 2015), DM25-

269   3 was tested for its binding activity to both mD2VLP and imD2VLP using antigen-capture

270   ELISA. MAb DM25-3 recognized mD2VLP very well, but reacted poorly with imD2VLP

271   (Figure 6C). Next, we performed site-directed mutagenesis on the fusion loop peptide in domain

272   II and A-strand in domain III, both of which are important binding regions for CR

273   group/complex neutralizing antibodies(de Alwis et al., 2011 ;Tsai et al., 2013) (Figure S12 in

274   Supplementary Material). The results suggested that amino acid E-101 was likely important in

275   the binding site of DM25-3. Residue 101 on the fusion loop of E protein is conserved among all

276   four serotypes of DENV and can only be exposed when virion particles undergo low-pH induced

277   conformational change or during the "breathing" state(Zhang et al., 2013b;Zhang et al., 2015).

278   Figure 3C shows that residue 101 is located at the touching point between EDII and EDIII of the

279   dimeric molecule. Since residue 101 is a critical residue in stabilizing E-protein dimers on

280   DENV virion, mutation on 101 would disrupt viral particle formation(Zhang et al.,

281   2013a;Rouvinski et al., 2017). However, mD2VLP with a mutation of residue 101 can still form

282   particles (Figure S13 in Supplementary Material), which further support our cryoEM model that

283   the E:E protein interactions on VLP are loose. When the E:E protein interaction was looser,

284   residue 101 at the groove within the dimeric molecule was more exposed (64%) than on the

285   native virion (23.8%, PDB:3J27) or on the native virion during the 37°C "breathing" state

286   (45.3%, PDB:3ZKO). We also generated a recombinant virus of DENV-2 whose EDIII was

287   exchanged for a consensus EDIII(Chen et al., 2013) and the recombinant virus PL046cEDIII was

288   recovered from the transfected cell culture supernatants for use in ELISA and FRμNT.

14

289   Compared to the parental DENV-2 strain PL046, there was significant loss of binding of MAb

290   DM25-3 and immune mouse sera to PL046cEDIII (Figure 6D), suggesting that DM25-3 could be

291   an E-dimer inter-domain antibody whose binding footprint is sensitive to amino acid changes in

292   the EDIII domain. By comparing $FR\mu NT_{50}$ tests using murine antisera on both PL046 and

293   PL046cEDIII viruses, we found that anti-mD2VLP sera showed a greater difference in

294   neutralizing activity against PL046 and PL046cEDIII than did anti-imD2VLP sera, indicating a

295   greater conformational dependence for anti-mD2VLP-triggered neutralization (Figure 6E).

296

297   Single B cells from the spleens of mD2VLP or imD2VLP-vaccinated mice were sorted

298   into 96-well plates to better understand DENV-2 prM/E-specific B-cell repertoires (Figure 7A).

299   By analyzing the amino acid sequences of the RT-PCR products of the variable regions of Ig

300   heavy-chain (IgH) and light-chain (IgL) genes, the B-cell response from mD2VLP-immunized

301   mice was more complex than the imD2VLP-immunized animals, particularly the gene loci of

302   IgH (Figure 7B). The IgH and IgL genes from the DM25-3-producing hybridoma were also

303   analyzed and found to contain IgHV1-22*01 and IgKV3-12*01 (Figure S14 in Supplementary

304   Material), which were clonally expanded as shown in Figure 7B.

305

306   The major obstacle of dengue vaccine development is the lack of a suitable small animal

307   model to evaluate vaccine efficacy. Therefore, we decided to test whether the monovalent

308   mD2VLP immunogen could provide protection from a lethal dose challenge of heterologous

309   dengue virus serotypes using suckling mice developed in a previous study(Chang et al.,

15

310   2003;Hughes et al., 2012;Galula et al., 2014). The advantage of using sucking mice to test

311   vaccine efficacy is that the protection from dengue virus challenge can only come from maternal

312   antibodies generated by vaccinated female mice and passively transferred to the their babies. The

313   immunization and challenge schedule is illustrated in Figure 8A. As shown in Figure 8B,

314   suckling mice born from mothers vaccinated with mD2VLP were all protected from challenge

315   with all four serotypes of dengue virus.

316

317

16

318 **Discussions**

319   How VLP immunogens mimic their viral counterparts structurally and how the

320 neutralizing epitopes are preserved on the VLP surface are of significant interest in the

321 development of good vaccine candidates. Recent studies suggest that potent human neutralizing

322 antibodies with broad reactivity across dengue serocomplex can be generated from dengue

323 patients, particularly after secondary infection(Tsai et al., 2013;Dejnirattisai et al.,

324 2015;Rouvinski et al., 2015). Our unique findings here suggested that mD2VLP, with a

325 scaffolding of multiple E-protein dimers similar to that of virion, is capable of inducing such CR

326 antibodies with broad neutralizing activity. This monovalent mature-form dengue VLP with

327 "epitope re-surfaced" has the potential to be the "epitope-focused" antigens when combined with

328 other live attenuated dengue vaccine to induce higher and broader neutralizing

329 antibodies(Rouvinski et al., 2017;Rey et al., 2018).

330

331   Very few studies explored the immunogenicity of prM-reduced antigens and its

332 capability in inducing broad NtAbs(Keelapang et al., 2013;Suphatrakul et al., 2015;Metz et al.,

333 2017;Rouvinski et al., 2017). Similar design of prM-reduced D2VLP was used as immunogens

334 but was produced from mosquito cells and such VLP required adjuvants to boost

335 immunity(Suphatrakul et al., 2015). Other attempts using E-dimers without the co-expression of

336 prM cannot only display the quaternary structure epitopes but also reduce the exposure of FLE

337 epitopes(Metz et al., 218;Metz et al., 2017;Rouvinski et al., 2017). However, the

338 immunogenicity of such E-dimers with only two copies of E could be lower than VLP. The

339 mD2VLP used in this study was produced from mammalian cells with the features similar to

17

340 dengue virion, such as glycosylation pattern, particle distribution in gradient after high-speed

341 centrifugation, epitopes preserved on the surface by the mapping of monoclonal antibodies, and

342 mostly importantly, multiple copies of E structurally packed as dimers on the particle surface

343 lattice (Fig S2 and S8 in Supplementary Material). Compared to imD2VLP (35%), only 7.6% of

344 prM-recognizing antibodies were induced by mD2VLP through 2H2-blocking assay. Current

345 dengue vaccine candidates in the market such as CYD-TDV or others in clinical trial are either

346 prM-possessing forms or E-protein monomer which is lack of quaternary epitopes(Wichmann et

347 al., 2017). Our study suggested that mD2VLP has the potential to be a safer immunogen as the

348 second-generation dengue vaccine.

349

350   In addition, mD2VLP-vaccinated mice produce antisera predominantly composed of

351 about 48% of DM25-3-like antibodies (Figure S15 in Supplementary Material). The packing of E

352 dimers on VLPs does not just preserve quaternary structure epitopes on the surface lattice as

353 suggested previously (Metz et al., 218;Crill et al., 2009), but also provides a unique surface-

354 accessible structure with increased epitope accessibility. Usually these epitopes are cryptic in

355 mature virions maintained at $28^{o}C$ and in a neutral-pH environment(Lok, 2016). By

356 superimposing the E-dimer-dependent quaternary epitopes(Lok et al., 2008;Fibriansah et al.,

357 2015a;Rouvinski et al., 2015) onto the structure of mD2VLP, the binding footprints of these

358 antibodies were highly overlapping and formed a "neutralization-sensitive hotspot" on mD2VLP

359 (Figure S16 in Supplementary Material). Thus, the underlying mechanisms of why mD2VLPs

360 are able to stimulate an elevated and broader immune response are based on the following: (1)

361 epitope accessibility exposed at the grooves within E-protein dimers, which govern the

18

362 generation of neutralizing antibodies; (2) removal of decoy epitopes presented on prM-

363 containing structures found in imD2VLPs; and (3) inter-dimeric epitope accessibility due to the

364 5-fold and 3-fold openings of the E protein arrangement of T=1. Other mechanisms cannot be

365 excluded such as reducing the production of FLE-like antibodies (ie. MAb E53), which have a

366 preference of binding to spikes on noninfectious, immature flavivirions by engaging the highly

367 conserved fusion loop that has limited solvent exposure of the epitope on mature virions(Cherrier

368 et al., 2009).

369

370 Although the current obstacle in developing the second generation dengue vaccine is that

371 dengue vaccine-induced neutralizing antibodies failed to correlate with or predict vaccine

372 mediated protection(Moodie et al., 2018;Yang et al., 2018). However, studies of vesicular

373 stomatitis virus demonstrated that *in vivo* protection depended on minimum serum antibody

374 concentration, regardless of immunoglobulin subclass, avidity or in vitro neutralization

375 activity(Bachmann et al., 1997). Therefore, it is crucial to understand the type of neutralizing

376 antibodies induced by vaccination and establish the association between the level of such

377 neutralizing antibodies and protection(Flipse and Smit, 2015;Henein et al., 2017;Katzelnick et al.,

378 2017). Recent studies suggested that the most potent neutralizing antibodies came from those

379 recognizing quaternary epitopes on the smooth surface of dengue virions(Fibriansah et al.,

380 2015b;Rouvinski et al., 2015;Crowe, 2017), Regardless of the mechanisms involved in NtAb

381 generation and protection from viral challenges, we have found that a mature form of

382 monovalent VLP from dengue virus serotype 2 with "epitope re-surfaced" is efficient in inducing

383 elevated and broadly NtAbs. When combined delivery with other live attenuated vaccine, such as

384   CYD-TDV or dengue tetravalent vaccine, there is potential to provide not just T-cell immunity,

385   but also higher broad NtAb response through "epitope-focusing" while exploring the next

386   generation dengue vaccine in humans(Crill et al., 2012;Flipse and Smit, 2015;Rey et al., 2018).

387

388   Our unique findings in this study showed that a mature, monovalent DENV-2 VLP with

389   grooves within the E protein dimeric molecules on the surface of particles induced highly

390   protective, NtAbs against heterologous dengue viruses from all four serotypes. These

391   characteristics strongly suggested this VLP with novel structure can combine with other live

392   attenuated dengue vaccine as "immune-focused" antigens to induce higher and broader

393   neutralizing antibodies. The strategy here may also provide a new direction for the development

394   of other flavivirus vaccines, including Zika virus.

395

396

397 **Materials and Methods**

398 Ethics statement

399 This study was carried out in compliance with the guidelines for the care and use of laboratory

400 animals of the National Laboratory Animal Center, Taiwan. The animal use protocol has been

401 reviewed and approved by the Institutional Animal Care and Use Committee (IACUC) of

402 National Chung Hsing University (Approval Number: 101-58). All efforts were made to

403 minimize suffering of mice.

404

405 Viruses, cells and antibodies

406 The strains of DENV serotypes 1-4 used were Hawaii (Genbank accession: KM204119.1),

407 16681 (Genbank accession: KU725663.1), H87 (Genbank accession: KU050695.1) and H241

408 (Genbank accession: AY947539.1), respectively. COS-1 (ATCC: CRL 1650), Vero (ATCC:

409 CRL 1587) and C6/36 cells (ATCC: CRL 1660) were grown in Dulbecco's modified Eagle's

410 medium (DMEM, Gibco, Life Technologies, Grand Island, NY) and were supplemented with

411 10% heat-inactivated fetal bovine serum (FBS, Hyclone, ThermoFisher, MA), 0.1mM

412 nonessential amino acids (Gibco, Life Technologies, Grand Island, NY), 7.5% $NaHCO_3$,

413 100U/ml penicillin, and 100ug/ml streptomycin; 5% FBS was used for Vero cells. Cells were

414 maintained at $37^{o}C$ with 5% CO_2, except for C6/36 cells, which were maintained at $28^{o}C$ without

415 CO_2. Parental DENV-2 strain PL046, generated from an infectious clone, and the domain III-

416 swapped PL046 (PL046cEDIII), with domain III of DENV-2 replaced by consensus sequence as

21

417   described previously (Liang et al., 2009;Chen et al., 2013), were provided by one of the co-

418   authors, Dr. Y-L Lin.

419   Murine monoclonal antibody (MAb) 2H2, recognizing DENV prM protein, group cross-

420   reactive antibodies (4G2, 4A1B-9, 6B3B-3, 6B6C-1, 5H3) recognizing E-protein of all four

421   major pathogenic flavivirus serocomplexes; complex cross-reactive antibodies (T5-1)

422   recognizing all four DENV serocomplex viruses; serotype-specific MAb 3H5-1, recognizing

423   DENV-2 only; rabbit sera and mouse hyper-immune ascitic fluid (MHIAF) for DENV-1 to 4

424   were provided by one of the authors, G-J Chang (DVBD, CDC, Fort Collins, CO). DENV-2 E

425   protein-specific MAb 32-6 was provided by Dr. H-C Wu (Academia Sinica, TW), while DENV-

426   2 prM-specific MAb 155-49 was obtained from H-Y Lei (National Cheng Kung University,

427   Taiwan). MAb 2H2 was also labeled with biotin using EZ-Link™ Sulfo-NHS-Biotin kit

428   (Thermo Fisher Scientific Inc., Rockford, IL) according to the manufacturer's instructions. In

429   order to increase the recognition of M protein, anti-M antibody was produced by cloning the

430   complete M protein sequence into pET21a (Novagen, Germany) and then purifying the

431   expressed protein under denaturing conditions as described in the molecular cloning handbook.

432   Ten micrograms (10μg) of purified M protein with Freud's complete adjuvant was used to

433   immunize the mice by the intraperitoneal route five times at 2-week intervals. Anti-mouse

434   CD45R/B220 antibody conjugated with APC (allophycocyanin) and goat anti-mouse IgG

435   conjugated with PE (phycoerythrin) were purchased from BioLegend (San Diego, CA).

436   Previously constructed and characterized recombinant plasmid pVD2, expressing the prM,

437   80% and 20% COOH terminus of the envelope proteins of DENV-2 (Asian 1 genotype, strain

438   16681) and Japanese encephalitis virus (strain SA14-14-2), respectively (Galula et al., 2014),

439   was used in this study. The furin cleavage site of prM was mutated in pVD2 to generate a prM-

440   uncleaved plasmid or as indicated in Figure 1A by using site-directed mutagenesis following the

441   manufacturer's protocol (Stratagene, La Jolla, CA). The primers used for cloning and site-

442   directed mutagenesis are provided in Table S1. Nucleotide sequencing confirmed that all the

443   plasmids contained no other mutations other than those indicated.

444

445   Sequence analysis of flavivirus prM sites

446   Flavivirus prM protein amino acid sequence alignments were performed using ClustalX

447   2.1 software with the representative strains and the GenBank accession numbers as follows:

448   dengue virus serotype 2 (NP_056776), dengue virus serotype 1 (AIU47321), dengue virus

449   serotype 3 (YP_001621843), dengue virus serotype 4 (NP_073286), Japanese encephalitis virus

450   (NP_775664), St. Louis encephalitis virus (AIW82235), West Nile virus (AIO10814), tick-borne

451   encephalitis virus (NP_775501), yellow fever virus (NP_041726), cell-fusion agent virus

452   (NP_041725), Zika virus (BAP47441.1). Sequences of prM junction region were scored for their

453   predicted cleavability by furin using the PiTou 2.0 software package(Tian et al., 2012). A

454   negative score indicates a sequence predicted not to be cleaved by furin, whereas a positive score

455   denotes prediction of furin cleavability.

456

457   Antigen production and purification

458   To produce virus-like particle (VLP) antigens, COS-1 cells at a density of 1.5×10^7

459   cells/mL were electroporated with 30 μg of each pVD2 plasmid following the previously

23

460   described protocol (Chang et al., 2000). After electroporation, cells were seeded into 75-cm^2

461   culture flasks (Corning Inc., Corning, NY, USA) containing 15 mL growth medium and allowed

462   to recover overnight at 37°C. The growth medium was replaced the next day with a maintenance

463   medium containing serum-free medium (SFM4MegaVirTM, SH30587.01, Hyclone,

464   ThermoFisher) supplemented with non-essential amino acid (NEAA), GlutaMAX, sodium

465   pyruvate and cholesterol (Gibco, Life Technologies, Grand Island, NY), and cells were

466   continuously incubated at 28°C with 5% CO_2 for VLP secretion. Tissue-culture media were

467   harvested 3 days after transfection and clarified by centrifugation at 8,000×g for 30 minutes

468   (mins) at 4°C in AF-5004CA rotor (Kubota, Tokyo, Japan) using a Kubota 3740 centrifuge. The

469   harvested media were first concentrated 20-fold using 100K Amicon Ultra centrifugal filters

470   (Merck Millpore, CA) before loading onto a 20% sucrose cushion and concentrated by

471   ultracentrifugation at 28,000 rpm for 16 hours at 4°C in a Beckman SW28 rotor. Purified VLPs

472   were resuspended in 250μl TNE buffer (50mM Tris-HCl, 100mM NaCl, 0.1 mM EDTA, pH 7.4)

473   for every liter of harvested medium at 4°C overnight. The VLPs were further purified by rate

474   zonal centrifugation in a 5 to 25% sucrose gradient at 25,000 rpm at 4°C for 3 hours. All

475   gradients were made with TNE buffer and were centrifuged in a Beckman SW41 rotor. Fractions

476   of 0.5 ml were collected by upward displacement and assayed by antigen-capture ELISA. For

477   experiments that required highly purified VLPs, proteins with the peak OD values from antigen-

478   capture ELISA were pelleted at 40,000 rpm at 4°C for 4 hours using a Beckman SW41 rotor, and

479   re-suspended in 250μl TNE buffer. The protein concentration was measured by the Bradford

480   assay (BioRad, Hercules, CA) following the commercial protocol and using bovine serum

481   albumin (BSA, New England Biolabs, MA) as a standard. Purified VLPs were also labeled with

482   fluorescein for antigen-specific B-cell sorting following the manufacture's protocol(Zhang et al.,

483   2010).

484

485   ELISA

486   The ratio of prM to E protein was determined using DENV-2 immune rabbit serum to

487   capture VLPs. The DENV-2 E and prM proteins were measured by ELISA using MAb 3H5

488   (specific for DENV-2 domain III) and MAb 155-49 (specific for DENV prM). The ratio was

489   calculated as absorbance for prM/absorbance for E protein. The uncleaved prM VLP

490   (imD2VLP), which contained amino acid mutations at P1 and P2 sites from amino acid residue

491   R/K to T/S (Li et al., 2008), respectively, was used as a standard to calculate the percentage of

492   prM cleavage. Percent cleavage of prM was then calculated with reference to imD2VLP, which

493   was assumed to be 100% uncleaved, as previously described (Dejnirattisai et al., 2015).

494

495   Antigen-capture ELISA was performed to quantify the amount of different VLP antigens.

496   Briefly, flat-bottom 96-well MaxiSorp™ NUNC-Immuno plates (NUNC™, Roskilde, Denmark)

497   were coated with 50 µL of rabbit anti-DENV-2 VLP serum at 1:500 in bicarbonate buffer (0.015

498   M Na_2CO_3, 0.035 $NaHCO_3$, pH 9.6), incubated overnight at 4°C, and blocked with 200 µL of 1%

499   BSA in PBS (1% PBSB) for 1 hr at 37°C. Clarified antigens were titrated two-fold in PBSB,

500   and 50 µL of each dilution was added to wells in duplicate, incubated for 2 hrs at 37°C, and

501   washed five times with 200 µL of 1x PBS with 0.1% Tween-20 (0.1% PBST). Normal COS-1

502   cell tissue culture fluid and cell pellets were used as control antigens. Captured antigens were

25

503   detected by adding 50 μL of anti-DENV-2 MHIAF at 1:2,000 in blocking buffer, incubated for 1

504   hr at 37°C, and washed for five times. Fifty microliters of HRP-conjugated goat anti-mouse IgG

505   (Jackson ImmunoResearch, Westgrove, PA, USA) at 1:5,000 in blocking buffer was added to

506   wells and incubated for 1 hr at 37°C to detect MHIAF. Subsequently, plates were washed ten

507   times. Bound conjugate was detected with 3,3',5,5'-tetramethylbenzidine substrate (Enhanced K-

508   Blue® TMB, NEOGEN® Corp., Lexington, KY, USA), after incubation at room temperature for

509   10 mins, and addition of 2N H_2SO_4 to stop the reaction. Reactions were measured at A_{450} using

510   a Sunrise™ TECAN microplate reader (Tecan, Grödig, Austria). The capability of antigen-

511   capture ELISA to detect imD2VLP or mD2VLP was measured against purified D2VLP at

512   known total protein concentration from individual preparations. Data are expressed as P/N ratio

513   by dividing the OD450 value from each dilution of mouse sera or MAb by the OD450 value

514   from the control COS-1 culture supernatant.

515

516   An IgG ELISA was used to assay the presence of antigen-specific IgG in the post-

517   vaccination mouse sera using the same antigen-capture ELISA protocol described above with

518   minor modifications. Equal amounts of purified antigens were added into each well of an Ag-

519   capture ELISA plate. The concentration of purified antigens were determined from the standard

520   curves generated using a sigmoidal dose-response analysis using GraphPad Prism (version 6.0,

521   GraphPad Software, Inc., La Jolla, CA, USA). Individual mouse sera, collected from mice

522   which had the same immunization schedule, initially diluted at 1:1,000, were titrated two-fold

523   and added into wells in duplicate, and were incubated for 1 hr at 37°C. Pre-vaccination mouse

524   sera were used as negative controls. Incubations with conjugate and substrate were carried out

525   according to the standard Ag-capture ELISA as outlined. The OD_{450} values, modeled as non-

526   linear functions of the log10 serum dilutions using a sigmoidal dose-response (variable slope)

527   equation and endpoint antibody titers from two independent experiments, were determined as the

528   dilutions where the OD value was twice the average OD of a negative control.

529

530   Epitope-blocking ELISAs were performed to determine the vaccinated mouse response to

531   the prM protein. The setup was similar to the IgG ELISA wherein plates were coated with rabbit

532   anti-DENV-2 VLP serum, and blocked with 1% BSA in PBS. After washing, pooled mouse sera

533   were diluted two-fold in blocking buffer starting from 1:1,000, and were then incubated with

534   imD2VLP antigen (pre-titrated to OD_{450}=1.0) for 1 hr at 37°C. After serum incubation and

535   washing, MAb 2H2 conjugated with biotin by EZ-Link Sulfo-NHS-Biotin (ThermoFisher, CA)

536   at 1:4000 dilution was added to each well and incubated for 1 hr at 37°C to compete with the

537   already-bound antibody from the immune mouse sera specific for the imD2VLP antigen. Bound

538   MAb 2H2 conjugate was detected with 1:1000 HRP-conjugated streptavidin (016-030-084,

539   Jackson ImmunoResearch), and was incubated for 1 hr at 37°C. After washing with PBS for ten

540   times, TMB substrate was added into the wells and the plates were incubated for 10 mins, and

541   the reaction was stopped with 2 N H_2SO_4. Reactions were measured at A_{450}. Percent blocking

542   was determined by comparing replicate wells with Biotin-conjugated MAb competing against

543   pre-adsorbed naïve mouse serum using the formula: % Blocking = [OD450 of imD2VLP-OD_{450}

544   of imD2VLP blocked by MAb 2H2)/OD_{450} of imD2VLP]×100.

545

546   Binding-ELISAs were used to assess the binding activity of MAbs or mouse immune sera

547   to D2VLP or mutant antigens using a similar antigen-capture ELISA set-up, except that two-fold

548   dilutions of the specific MAb or immune mouse sera replaced the anti-DENV-2 MHIAF. Equal

549   amounts of D2VLP antigens were added into wells, and were standardized using purified

550   D2VLPs. The antibody endpoint reactivity was determined in a similar manner to the

551   determination of antigen endpoint secretion titers.

552

553   SDS-PAGE and Western blotting

554   Equal amounts of purified VLPs and sample buffer were mixed and analyzed by 12%

555   Tricine-sodium   dodecyl   sulfate-polyacrylamide   gel   electrophoresis   (Tricine-SDS-

556   PAGE)(Schägger, 2006). For immunodetection, proteins were blotted from gels onto

557   nitrocellulose membranes (iBlot®2NC mini stacks, ThermoFisher Scientific) with iBlot® 2 Gel

558   Transfer Device (ThermoFisher Scientific). The membranes were incubated for 1 hour at room

559   temperature in phosphate-buffered saline (pH 7.4) containing 5% skim milk (BD biosciences,

560   CA) to block nonspecific antibody binding. After 1hr incubation, membranes were individually

561   stained to detect E, prM and M proteins by using anti-DENV2 MHIAF at 1:2000, anti-DENV

562   prM MAb 155-49 at 0.5μg/ml and mouse anti-M sera at 1:25, respectively, at 4°C overnight.

563   Membranes were washed three times for 15 min each. DENV-specific bound immunoglobulin

564   was recognized with HRP-labeled goat anti-mouse IgG (Jackson ImmunoReasearch, PA), and

565   was visualized with ECL (enhanced chemiluminescent substrate, GE Healthcare, UK) according

566   to the manufacturer's protocol. The ECL signals were detected by ImageQuant^{TM} LAS 4000

28

567   mini (GE Healthcare). However, M protein was visualized using TMB membrane peroxidase

568   substrate (KPL, MD) to avoid high background from ECL.

569

570   Mouse experiment

571   Groups of four 4-week-old female BALB/c mice were injected intramuscularly with

572   imD2VLP and mD2VLP at weeks 0 and 4 at a dose of 4 μg/100 μL PBS divided between the

573   right and left quadriceps muscle. Mice were bled from the retro-orbital sinus at week 4 following

574   the second injection, and individual serum specimens were evaluated for DENV-2 specific

575   antibodies by ELISA and focus-reduction micro-neutralization test (FRμNT), as described in the

576   following section.

577

578   For the evaluation of passive protection by maternal antibody, ICR pups from the mating

579   of non-immunized males with immunized females 11 weeks post initial vaccination were

580   obtained for viral challenge. Immune sera were collected from immunized females 1 week prior

581   to mating to confirm the presence of the total IgG titer as well as the virus neutralization

582   antibody titer. Pups from unvaccinated females were used as the challenge control. ICR pups

583   from the designated groups were challenged individually through the intracranial route at 2 days

584   after birth with 10^4 focus-forming units (FFU) which were equivalent to 141, 61, 11, 1000-fold

585   of 50% lethal doses (LD50) of DENV-1 (strain Hawaii), DENV-2 (strain 16681), DENV-3

586   (strain H87) and DENV-4 (strain BC71/94, kindly provided by one of the co-author, Dr. Chang

587   from US-CDC), respectively. Mouse survival was evaluated daily for up to 21 days.

588

589   Virus neutralization

590   The neutralizing ability of the immune mouse sera for all serotypes of DENV was

591   measured by focus-reduction micro neutralization test (FRµNT), as previously described(Galula

592   et al., 2014). Briefly, 2.475×10^4 Vero cells/well were seeded onto flat-bottom 96-well Costar$^®$

593   cell culture plates (Corning Inc., Corning, NY, USA) and incubated for 16 hrs overnight at 37°C

594   with 5% CO_2. Pooled sera were initially diluted at 1:10, heat-inactivated for 30 min at 56°C,

595   titrated two-fold to a 40 µL volume, and 320 pfu/40 µL of DENV-1 to 4 was added to each

596   dilution. The mixtures were then incubated for 1 hr at 37°C. After incubation, 25 µL of the

597   immune complexes were added in duplicates onto plates containing Vero cell monolayers. Plates

598   were incubated for 1 hr at 37°C with 5% CO_2 and rocked every 10 mins to allow infection.

599   Overlay medium containing 1% methylcellulose (Sigma-Aldrich Inc., St. Louis, MO, USA) in

600   DMEM with 2% FBS was added, and plates were incubated at 37°C with 5% CO_2. Forty-eight

601   hours later, plates were washed, fixed with 75% acetone in PBS and air-dried. Immunostaining

602   was performed by adding serotype-specific MHIAF at 1:600 in 5% milk and 0.1% PBST and

603   incubated for 60 min at 37°C. Plates were washed and goat anti-mouse IgG-HRP at 1:100 in 5%

604   milk and 0.1% PBST was added; plates were incubated for 45 min at 37°C. Infection foci were

605   visualized using a peroxidase substrate kit, Vector$^®$ VIP SK-4600 (Vector Laboratories, Inc.,

606   Burlingame, CA, USA), following the manufacturer's instructions. FRµNT titers were calculated

607   for each virus relative to a virus only control back-titration. Titers were determined as a 50%

608   reduction of infection foci (FRµNT50) and were modeled using a sigmoidal dose-response

609   (variable slope) formula. All values were determined from the average of two independent

30

610   experiments. Target virus strains were: DENV-1, Hawaii; DENV-2, 16681; DENV-3, H87; and

611   DENV-4, H241. For E-dimer, inter-domain-specific neutralizing antibodies, the recombinant

612   parental DENV-2 strain PL046 and EDIII-swapped PL046cEDIII were used as target viruses. In

613   the calculation of geometric mean titers (GMT) for graphic display and statistical analysis, a

614   FRµNT50 titer of <10 was represented with the value of 1 and 5, respectively.

615

616   Generating hybridomas and MAb screening

617   Hybridomas secreting anti-DENV antibodies were generated from the mD2VLP

618   immunized mice according to a standard procedure(Kohler and Milstein, 1975), with slight

619   modifications(Chen et al., 2007). First, the mD2VLP-immunized mouse was boosted with

620   another 4µg of mD2VLP 24 weeks prior to terminal bleeding. At day 4 after the third

621   immunization, splenocytes were harvested from the immunized mouse and fused with NSI/1-

622   Ag4-1 myeloma cells using an antibody delivery kit following manufacturer's recommendations

623   (GenomONETM-CF HVJ Envelope Cell Fusion Kit, Gosmo Bio Co, ISK10 MA17). Fused cell

624   pellets were suspended in DMEM supplemented with 15% FBS, hypoxanthine-aminopterin-

625   thymidine medium, and hybridoma cloning factor (ICN, Aurora, OH). Hybridoma colonies were

626   screened for secretion of MAbs by ELISA following the procedures as described above.

627   However, the cell culture supernatant of C6/36 cells infected with DENV-2 virus at a

628   multiplicity of infection (moi) equal to 1.0 was used as the antigens and the culture supernatant

629   from each of the hybridoma colonies was used as the detecting antibody. Selected positive clones

630   were subcloned by limiting dilution. Ascitic fluids were produced in pristane-primed BALB/c

631   mice. Hybridoma cell lines were grown in DMEM with 10% heat inactivated FBS. MAbs were

632   affinity purified with protein G Sepharose 4B gel, and the amount of each purified MAb was

633   quantified by comparison with a known amount of IgG used in a standard ELISA.

634

635   Profiling of prM/E-specific Ig genes from a single B-cell

636   Ig genes from a single B cell were isolated following the protocols established by

637   previous reports with some modifications(Tiller et al., 2009). Briefly, single cell suspensions

638   were collected from the spleens of BALB/c mice immunized twice at 4-week intervals with

639   imD2VLP and mD2VLP. The D2VLP(+), B220 (+) and IgG1(+) splenic B cells were isolated

640   by flow cytometry (FACSAria II), and single B cells were sorted into 96-well PCR plates

641   containing 4ul/well of ice-cold RNase-free water supplemented with 10mM DTT and 3U RNase

642   inhibitor (Promega). RT-PCR reactions were performed using the Qiagen OneStep RT-PCR kit

643   (Qiagen) at 50°C for 30 mins and at 95°C for 15 min followed by 40 cycles of 95°C for 1 min,

644   55°C for 1 min and 72°C 1 min, and a final incubation at 72°C for 5 min, with the primers as

645   previously described. The nested PCR was performed using 2 ul of unpurified, first-round PCR

646   product at 95°C for 1 min followed by 40 cycles of 95°C 30 sec, 57°C (IgH) or 45°C (Igk) or

647   55°C (Igλ) for 30sec, 72°C for 45sec, and incubated at 72°C for 10 min as previously described.

648   Aliquots of nested PCR products were sequenced and analyzed using IMGT/V-Quest

649   (http://www.imgt.org) to identify the highest homology gene loci of germ-line V, D and J genes.

650   Ig genes were then translated and aligned by CLUSTALW to define the clonally amplified Ig

651   genes.

652

653   Immunogold labeling and transmission electron microscopy (TEM)

654   To detect mature DENV-2 VLPs (mD2VLPs) as spherical particles, 3μL of freshly

655   prepared samples were adsorbed onto a glow-discharged nickel grid (EMS CF-200-Ni) for 20

656   mins, The grid containing the samples was incubated in 1% BSA/PBS blocking buffer for 1 hour

657   at room temperature. As soon as the excess liquid was removed with a filter paper, DENV-2-

658   specific MAb DB32-6 was used as the primary antibody (dilution 1:500), and was added to the

659   samples for 2 hrs at room temperature. Then the grid was washed with blocking buffer and

660   incubated with 6-nm nanogold-conjugated Donkey anti-mouse IgG (Abcam, MA) (dilution 1:30)

661   at room temperature for 1 hr. The excess liquid was removed with filter paper and fixed with 1%

662   glutaraldehyde in PBS buffer (GA/PBS) for 10 mins. After fixing, excess liquid was removed

663   using a filter paper. Finally, the sample was stained with 2% uranyl acetate (UA) for 1 min and

664   air-dried. The immunogold labeling process was performed in a high humidity chamber. The

665   immunogold labeled mD2VLPs were inspected by TEM. The images were taken by a JEM1400

666   electron transmission microscope at a magnification of 100,000x using a 4k x 4k Gatan 895 CCD

667   camera. The diameters of particles were measured by ImageJ software.

668

669   Cryo-EM and 3D reconstruction

670   A freshly prepared dengue virus sample (3 μl) was placed onto a glow-discharged

671   Quatifoil 2/2 grid (Quatifoil GmbH, Germany), blotted with filter paper, and plunged into liquid

672   nitrogen-cooled liquid ethane using Gatan CP3. Cryo-EM images were recorded with a

673   JEM2100F using an accelerating voltage of 200kV and a magnification of 15,000x using a direct

33

674 electron detector (DE-12 Camera System - Direct Electron, LP) with a 6 μm pixel size

675 (corresponding to ~4 Å at the specimen level). The measured defocus values of these images

676 range from −2μm to −4.5μm. The imaging electron dosage was ~ 10 e⁻/Å² .

677

678   Variations in size and shape were observed in the EM images (Figure S3A, B in

679 Supplementary Material). The irregularly-shaped particles were eliminated through visual

680 inspection, while the spherical particles were subjected to further image analyses. The particle

681 size analyses showed that the major peaks were located at ~26nm, ~31nm and ~36nm diameter

682 size classes which were therefore denoted by small ('S'), medium ('M') and large ('L'). The

683 heterogeneity analyses by EMAN2(Tang et al., 2007) and XMIPP(Sorzano et al., 2004;de la

684 Rosa-Trevín et al., 2013) showed that all of the classes had distinct two layers and that the

685 particles classes with diameters of 31nm had more prominent features than others (Figure S3B, C

686 in Supplementary Material). Taken together with the immunogold labeling results, we selected

687 the particles with size of ~31nm or further 3D reconstruction process. The structure

688 reconstruction processes were performed by EMAN2. There were 4,217 spherical particles with

689 the size of ~31nm which were included in the reconstruction process and the icosahedral

690 symmetry was imposed during the whole process. The reconstruction process ended when there

691 was no improvement achieved. The resolution of the final reconstructions was 13.1Å from a

692 Fourier shell correlation curve using the gold standard resolution estimate in EMAN2 (Figure S5

693 in Supplementary Material). Solvent accessible surface area (SASA) of individual amino acid

694 molecules on mD2VLP was calculated by POPS program(Cavallo et al., 2003;Fornili et al.,

695 2012).

696

697   Fitting

698   The atomic structure of mD2VLP was modeled based on the cryo-EM structure of the

699   mature dengue virus at 3.5Å resolution (PDB ID: 3J27) using MODELLER 9v15(Eswar et al.,

700   2007). The envelop proteins were fitted rigidly using the Fit-in-Map tool in *UCSF Chimera,*

701   when the CCC (Cross-Correlation Coefficient) score was maximized, the complete copies were

702   generated to follow the T=1 arrangement with *Multiscale Models* using Icosahedral symmetry,

703   xyz 2-fold axes (VIPER).

704

705   Statistical analysis

706   All data are represented as means ± standard error, and analyzed using GraphPad Prism

707   version 6.0. Unpaired t test was used to analyze data sets between two groups. Mann-Whitney U

708   test to account for non-normality of some transformed data was also applied. P values <0.05

709   were considered significant.

710

711

712   **Data and materials availability**

713   The cryo-EM density map of mD2VLP has been deposited to Electron Microscopy Data Bank

714   under accession number EMDB6926. All other relevant data are available from the authors on

715   request.

35

716

717

Acknowledgments:

We thank Dr. Felix Rey for commenting on the structure of dengue VLP and Ann Hunt for English editing.

721

Author contributions: WFS performed the characterization of D2VLP including Western blotting, ELISA, site-directed mutagenesis and mouse immunization. JHL conducted the Pitou and solvent accessibility analysis. MYL, DYC, HCW and JUG produced and characterized the NS1-splenocytes fused B cell lines, monoclonal antibody and single B-cell repertoire characterization. WFS and YCW conducted VLP purification, mouse immunization experiments and neutralization assays. JUG and CHH prepared the anti-M protein mouse polyclonal serum. JJL and YLL prepared the parental and domain III-replaced recombinant DENV-2. SRC and SRW prepared the cryo-EM samples, processed the cryo-EM images, fitted the protein structures, and solved the cryo-EM structure. MTW, GJC and WFS mapped the 2H2 binding epitopes. SRW, GJC and DYC supervised the studies and contributed to the writing of the paper.

732

Competing interests: All the authors declare that they have no competing interests.

734

36

737

738

739

References

Aguiar, M., Stollenwerk, N., and Halstead, S. (2016). The Impact of the Newly Licensed Dengue Vaccine in Endemic Countries. *PLoS Negl Trop Dis* 10**,** e0005179.

Allison, S., Stadler, K., Mandl, C., Kunz, C., and Heinz, F. (1995). Synthesis and secretion of recombinant tick-borne encephalitis virus protein E in soluble and particulate form. *J Virol* 69**,** 5816-5820.

Bachmann, M., Kalinke, U., Althage, A., Freer, G., Burkhart, C., Roost, H., Aguet, M., Hengartner, H., and Zinkernagel, R. (1997). The role of antibody concentration and avidity in antiviral protection. *Science* 276**,** 2024-2027.

Bhatt, S., Gething, P., Brady, O., Messina, J., Farlow, A., Moyes, C., Drake, J., Brownstein, J., Hoen, A., Sankoh, O., Myers, M., George, D., Jaenisch, T., Wint, G., Simmons, C., Scott, T., Farrar, J., and Hay, S. (2013). The global distribution and burden of dengue. *Nature* 496**,** 504-507.

Cavallo, L., Kleinjung, J., and Fraternali, F. (2003). POPS: A fast algorithm for solvent accessible surface areas at atomic and residue level. *Nucleic Acids Res* 31**,** 3364-3366.

Chambers, T.J., Hahn, C.S., Galler, R., and Rice, C.M. (1990). Flavivirus genome: organization, expression and replication. *Annu. Rev. Microbiol.* 44**,** 649-688.

Chang, G.-J.J., Hunt, A.R., Holmes, D.A., Springfield, T., Chiueh, T.S., Roehrig, J.T., and Gubler, D.J. (2003). Enhancing biosynthesis and secretion of premembrane and envelope proteins by the chimeric plasmid of dengue virus type 2 and Japanese encephalitis virus. *Virology* 306**,** 170-180.

Chang, G., Hunt, A., and Davis, B. (2000). A single intramuscular injection of recombinant plasmid DNA induces protective immunity and prevents Japanese encephalitis in mice. *J Virol* 74**,** 4244-4252.

Chen, H., Liu, S., Li, Y., Liu, H., Tsai, J., Chiang, C., Chen, M., Hwang, C., Huang, C., Hu, H., Chung, H., Wu, S., Chong, P., Leng, C., and Pan, C. (2013). A consensus envelope protein domain III can induce neutralizing antibody responses against serotype 2 of dengue virus in non-human primates. *Arch Virol* 158**,** 1523-1531.

Chen, Y., Huang, H., Lin, C., Chen, Y., King, C., and Wu, H. (2007). Generation and characterization of monoclonal antibodies against dengue virus type 1 for epitope mapping and serological detection by epitope-based peptide antigens. *Clin Vaccine Immunol* 14**,** 404-411.

Cherrier, M., Kaufmann, B., Nybakken, G., Lok, S., Warren, J., Chen, B., Nelson, C., Kostyuchenko, V., Holdaway, H., Chipman, P., Kuhn, R., Diamond, M., Rossmann, M., and Fremont, D. (2009). Structural basis for the preferential recognition of immature flaviviruses by a fusion-loop antibody. *EMBO J* 28**,** 3269-3276.

Crill, W., Hughes, H., Delorey, M., and Chang, G. (2009). Humoral immune responses of dengue fever patients using epitope-specific serotype-2 virus-like particle antigens. *PLoS One* 4**,** e4991.

Crill, W.D., Hughes, H.R., Trainor, N.B., Davis, B.S., Whitney, M.T., and Chang, G.J. (2012). Sculpting humoral immunity through dengue vaccination to enhance protective immunity. *Front Immunol* 3**,** 334.

Crowe, J.J. (2017). Principles of Broad and Potent Antiviral Human Antibodies: Insights for Vaccine Design. *Cell Host Microbe* 22**,** 193-206.

Da Silva Voorham, J., Rodenhuis-Zybert, I., Ayala Nuñez, N., Colpitts, T., Van Der Ende-Metselaar, H., Fikrig, E., Diamond, M., Wilschut, J., and Smit, J. (2012). Antibodies against the envelope glycoprotein promote infectivity of immature dengue virus serotype 2. *PLoS One* 7**,** e29957.

De Alwis, R., Beltramello, M., Messer, W., Sukupolvi-Petty, S., Wahala, W., Kraus, A., Olivarez, N., Pham, Q., Brien, J., Tsai, W., Wang, W., Halstead, S., Kliks, S., Diamond, M., Baric, R., Lanzavecchia, A., Sallusto, F., and De Silva, A. (2011). In-depth analysis of the antibody response of individuals exposed to primary dengue virus infection. *PLoS Negl Trop Dis* 5**,** e1188.

De La Rosa-Trevín, J., Otón, J., Marabini, R., Zaldívar, A., Vargas, J., Carazo, J., and Sorzano, C. (2013). Xmipp 3.0: an improved software suite for image processing in electron microscopy. *J Struct Biol* 184**,** 321-328.

Dejnirattisai, W., Jumnainsong, A., Onsirisakul, N., Fitton, P., Vasanawathana, S., Limpitikul, W., Puttikhunt, C., Edwards, C., Duangchinda, T., Supasa, S., Chawansuntati, K., Malasit, P., Mongkolsapaya, J., and Screaton, G. (2010). Cross-reacting antibodies enhance dengue virus infection in humans. *Science* 328**,** 745-748.

Dejnirattisai, W., Wongwiwat, W., Supasa, S., Zhang, X., Dai, X., Rouvinski, A., Jumnainsong, A., Edwards, C., Quyen, N., Duangchinda, T., Grimes, J., Tsai, W., Lai, C., Wang, W., Malasit, P., Farrar, J., Simmons, C., Zhou, Z., Rey, F., Mongkolsapaya, J., and Screaton, G. (2015). A new class of highly potent, broadly neutralizing antibodies isolated from viremic patients infected with dengue virus. *Nat Immunol* 16**,** 170-177.

791 Eswar, N., Webb, B., Marti-Renom, M., Madhusudhan, M., Eramian, D., Shen, M., Pieper, U., and Sali, A. (2007).
792   Comparative protein structure modeling using MODELLER. *Curr Protoc Protein Sci* Chapter 2.

793 Ferlenghi, I., Clarke, M., Ruttan, T., Allison, S., Schalich, J., Heinz, F., Harrison, S., Rey, F., and Fuller, S. (2001).
794   Molecular organization of a recombinant subviral particle from tick-borne encephalitis virus. *Mol Cell* 7**,**
795   593-602.

796 Fibriansah, G., Ibarra, K., Ng, T., Smith, S., Tan, J., Lim, X., Ooi, J., Kostyuchenko, V., Wang, J., De Silva, A.,
797   Harris, E., Crowe, J.J., and Lok, S. (2015a). DENGUE VIRUS. Cryo-EM structure of an antibody that
798   neutralizes dengue virus type 2 by locking E protein dimers. *Science* 349**,** 88-91.

799 Fibriansah, G., Tan, J., Smith, S., De Alwis, R., Ng, T., Kostyuchenko, V., Jadi, R., Kukkaro, P., De Silva, A.,
800   Crowe, J., and Lok, S. (2015b). A highly potent human antibody neutralizes dengue virus serotype 3 by
801   binding across three surface proteins. *Nat Commun* 6.

802 Flipse, J., and Smit, J. (2015). The Complexity of a Dengue Vaccine: A Review of the Human Antibody Response.
803   *PLoS Negl Trop Dis* 9**,** e0003749.

804 Fornili, A., Autore, F., Chakroun, N., Martinez, P., and Fraternali, F. (2012). Protein-water interactions in MD
805   simulations: POPS/POPSCOMP solvent accessibility analysis, solvation forces and hydration sites.
806   *Methods Mol Biol* 819**,** 375-392.

807 Galula, J.U., Shen, W.F., Chuang, S.T., Chang, G.J., and Chao, D.Y. (2014). Virus-like particle secretion and
808   genotype-dependent immunogenicity of dengue virus serotype 2 DNA vaccine. *J Virol* 88**,** 10813-10830.

809 Guy, B., and Jackson, N. (2016). Dengue vaccine: hypotheses to understand CYD-TDV-induced protection. *Nat Rev*
810   *Microbiol* 14**,** 45-54.

811 Halstead, S. (2017). Dengvaxia sensitizes seronegatives to vaccine enhanced disease regardless of age. *Vaccine* 35**,**
812   6355-6358.

813 Henein, S., Swanstrom, J., Byers, A., Moser, J., Shaik, S., Bonaparte, M., Jackson, N., Guy, B., Baric, R., and De
814   Silva, A. (2017). Dissecting Antibodies Induced by a Chimeric Yellow Fever-Dengue, Live-Attenuated,
815   Tetravalent Dengue Vaccine (CYD-TDV) in Naive and Dengue-Exposed Individuals. *J Infect Dis* 215**,**
816   351-358.

817 Huang, K., Yang, Y., Lin, Y., Huang, J., Liu, H., Yeh, T., Chen, S., Liu, C., and Lei, H. (2006). The dual-specific
818   binding of dengue virus and target cells for the antibody-dependent enhancement of dengue virus infection.
819   *J Immunol* 76**,** 2825-2832.

820 Hughes, H., Crill, W., and Chang, G. (2012). Manipulation of immunodominant dengue virus E protein epitopes
821   reduces potential antibody-dependent enhancement. *Virol J* 9**,** 115.

822 Junjhon, J., Edwards, T., Utaipat, U., Bowman, V., Holdaway, H., Zhang, W., Keelapang, P., Puttikhunt, C., Perera,
823   R., Chipman, P., Kasinrerk, W., Malasit, P., Kuhn, R., and Sittisombut, N. (2010). Influence of pr-M
824   cleavage on the heterogeneity of extracellular dengue virus particles. *J Virol* 84**,** 8353-8358.

825 Katzelnick, L., Coloma, J., and Harris, E. (2017). Dengue: knowledge gaps, unmet needs, and research priorities.
826   *Lancet Infect Dis* 17**,** e88-e100.

827 Keelapang, P., Nitatpattana, N., Suphatrakul, A., Punyahathaikul, S., Sriburi, R., Pulmanausahakul, R., Pichyangkul,
828   S., Malasit, P., Yoksan, S., and Sittisombut, N. (2013). Generation and preclinical evaluation of a DENV-
829   1/2 prM+E chimeric live attenuated vaccine candidate with enhanced prM cleavage. *Vaccine* 31**,** 5134-
830   5140.

831 Kirkpatrick, B., Whitehead, S., Pierce, K., Tibery, C., Grier, P., Hynes, N., Larsson, C., Sabundayo, B., Talaat, K.,
832   Janiak, A., Carmolli, M., Luke, C., Diehl, S., and Durbin, A. (2016). The live attenuated dengue vaccine
833   TV003 elicits complete protection against dengue in a human challenge model. *Sci Transl Med* 8**,** 330ra336.

834 Kohler, G., and Milstein, C. (1975). Continuous cultures of fused cells secreting antibody of predefined specificity.
835   *Nature* 256**,** 495-497.

836 Kostyuchenko, V., Zhang, Q., Tan, J., Ng, T., and Lok, S. (2013). Immature and mature dengue serotype 1 virus
837   structures provide insight into the maturation process. *J Virol* 87**,** 7700-7707.

838 Li, L., Lok, S., Yu, I., Zhang, Y., Kuhn, R., Chen, J., and Rossmann, M. (2008). The flavivirus precursor membrane-
839   envelope protein complex: structure and maturation. *Science* 319**,** 1830-1834.

840 Li, P., Liao, M., Cheng, P., Liang, J., Liu, I., Chiu, C., Lin, Y., Chang, G., and Wu, H. (2012). Development of a
841   humanized antibody with high therapeutic potential against dengue virus type 2. *PLoS Negl Trop Dis* 6**,**
842   e1636.

843 Liang, J., Liao, C., Liao, J., Lee, Y., and Lin, Y. (2009). A Japanese encephalitis virus vaccine candidate strain is
844   attenuated by decreasing its interferon antagonistic ability. *Vaccine* 27**,** 2746-2754.

39

845 Lindenbach, B.D., and Rice, C.M. *"Flaviviridae*: The viruses and their replication." in *Fields' Virology*, D. M. Knipe
846   and P. M. Howley, Eds. (Lippincott Williams & Wilkins, Philadelphia, ed. 4, 2001). *pp.991-1110*, .
847 Lok, S. (2016). The interplay of dengue virus morphological diversity and human antibodies. *Trends Microbiol* 24**,**
848   284-293.
849 Lok, S.M., Kostyuchenko, V., Nybakken, G.E., Holdaway, H.A., Battisti, A.J., Sukupolvi-Petty, S., Sedlak, D.,
850   Fremont, D.H., Chipman, P.R., Roehrig, J.T., Diamond, M.S., Kuhn, R.J., and Rossmann, M.G. (2008).
851   Binding of a neutralizing antibody to dengue virus alters the arrangement of surface glycoproteins. *Nat
852   Struct Mol Biol* 15**,** 312-317.
853 Metz, S., Gallichotte, E., Brackbill, A., Premkumar, L., Miley, M., Baric, R., and De Silva, A. (2017). In Vitro
854   Assembly and Stabilization of Dengue and Zika Virus Envelope Protein Homo-Dimers. *Sci Rep* 7**,** 4524.
855 Metz, S., Thomas, A., White, L., Stoops, M., Corten, M., Hannemann, H., and De Silva, A. (218). Dengue virus-like
856   particles mimic the antigenic properties of the infectious dengue virus envelope. *Virol J* 15**,** 60.
857 Modis, Y., Ogata, S., Clements, D., and Harrison, S. (2003). A ligand-binding pocket in the dengue virus envelope
858   glycoprotein. *Proc Natl Acad Sci* 100**,** 6986-6991.
859 Moodie, Z., Juraska, M., Huang, Y., Zhuang, Y., Fong, Y., Carpp, L., Self, S., Chambonneau, L., Small, R., Jackson,
860   N., Noriega, F., and Gilbert, P. (2018). Neutralizing Antibody Correlates Analysis of Tetravalent Dengue
861   Vaccine Efficacy Trials in Asia and Latin America. *J Infect Dis* 217**,** 742-753.
862 Nelson, S., Jost, C., Xu, Q., Ess, J., Martin, J., Oliphant, T., Whitehead, S., Durbin, A., Graham, B., Diamond, M.,
863   and Pierson, T. (2008). Maturation of West Nile virus modulates sensitivity to antibody-mediated
864   neutralization. *PLoS Pathog* 4**,** e1000060.
865 Pierson, T., and Diamond, M. (2012). Degrees of maturity: the complex structure and biology of flaviviruses. *Curr
866   Opin Virol* 2**,** 168-175.
867 Pierson, T., Fremont, D., Kuhn, R., and Diamond, M. (2008). Structural insights into the mechanisms of antibody-
868   mediated neutralization of flavivirus infection: implications for vaccine development. *Cell Host Microbe* 4**,**
869   229-238.
870 Purdy, D., and Chang, G. (2005). Secretion of noninfectious dengue virus-like particles and identification of amino
871   acids in the stem region involved in intracellular retention of envelope protein. *Virology* 333**,** 239-250.
872 Rey, F., Stiasny, K., Vaney, M., Dellarole, M., and Heinz, F. (2018). The bright and the dark side of human antibody
873   responses to flaviviruses: lessons for vaccine design. *EMBO Rep* 19**,** 206-224.
874 Rodenhuis-Zybert, I., Da Silva Voorham, J., Torres, S., Van De Pol, D., and Smit, J. (2015). Antibodies against
875   immature virions are not a discriminating factor for dengue disease severity. *PLoS Negl Trop Dis* 9**,**
876   e0003564.
877 Rodenhuis-Zybert, I., Moesker, B., Da Silva Voorham, J., Van Der Ende-Metselaar, H., Diamond, M., Wilschut, J.,
878   and Smit, J. (2011). A fusion-loop antibody enhances the infectious properties of immature flavivirus
879   particles. *J Virol* 85**,** 11800-11808.
880 Rodenhuis-Zybert, I., Van Der Schaar, H., Da Silva Voorham, J., Van Der Ende-Metselaar, H., Lei, H., Wilschut, J.,
881   and Smit, J. (2010). Immature dengue virus: a veiled pathogen? *PLoS Pathog* 6**,** e1000718.
882 Roehrig, J.T. (2003). Antigenic structure of flavivirus proteins. *Adv Virus Res.* 59**,** 141-175.
883 Rouvinski, A., Dejnirattisai, W., Guardado-Calvo, P., Vaney, M., Sharma, A., Duquerroy, S., Supasa, P.,
884   Wongwiwat, W., Haouz, A., Barba-Spaeth, G., Mongkolsapaya, J., Rey, F., and Screaton, G. (2017).
885   Covalently linked dengue virus envelope glycoprotein dimers reduce exposure of the immunodominant
886   fusion loop epitope. *Nat Commun* 8**,** 15411.
887 Rouvinski, A., Guardado-Calvo, P., Barba-Spaeth, G., Duquerroy, S., Vaney, M., Kikuti, C., Navarro Sanchez, M.,
888   Dejnirattisai, W., Wongwiwat, W., Haouz, A., Girard-Blanc, C., Petres, S., Shepard, W., Desprès, P.,
889   Arenzana-Seisdedos, F., Dussart, P., Mongkolsapaya, J., Screaton, G., and Rey, F. (2015). Recognition
890   determinants of broadly neutralizing human antibodies against dengue viruses. *Nature* 520**,** 109-113.
891 Schägger, H. (2006). Tricine-SDS-PAGE. *Nat Protoc* 1**,** 16-22.
892 Sorzano, C., Marabini, R., Velázquez-Muriel, J., Bilbao-Castro, J., Scheres, S., Carazo, J., and Pascual-Montano, A.
893   (2004). XMIPP: a new generation of an open-source image processing package for electron microscopy. *J
894   Struct Biol* 148**,** 194-204.
895 Suphatrakul, A., Yasanga, T., Keelapang, P., Sriburi, R., Roytrakul, T., Pulmanausahakul, R., Utaipat, U.,
896   Kawilapan, Y., Puttikhunt, C., Kasinrerk, W., Yoksan, S., Auewarakul, P., Malasit, P., Charoensri, N., and
897   Sittisombut, N. (2015). Generation and preclinical immunogenicity study of dengue type 2 virus-like
898   particles derived from stably transfected mosquito cells. *Vaccine* 33**,** 5613-5622.

899 Tang, G., Peng, L., Baldwin, P., Mann, D., Jiang, W., Rees, I., and Ludtke, S. (2007). EMAN2: an extensible image
900   processing suite for electron microscopy. *J Struct Biol* 157**,** 38-46.
901 Tian, S., Huajun, W., and Wu, J. (2012). Computational prediction of furin cleavage sites by a hybrid method and
902   understanding mechanism underlying diseases. *Sci Rep* 2**,** 261.
903 Tiller, T., Busse, C., and Wardemann, H. (2009). Cloning and expression of murine Ig genes from single B cells. *J*
904   *Immunol Methods* 350**,** 183-193.
905 Tsai, W., Lai, C., Wu, Y., Lin, H., Edwards, C., Jumnainsong, A., Kliks, S., Halstead, S., Mongkolsapaya, J.,
906   Screaton, G., and Wang, W. (2013). High-avidity and potently neutralizing cross-reactive human
907   monoclonal antibodies derived from secondary dengue virus infection. *J Virol* 87**,** 12562-12575.
908 Wang, Z., Li, L., Pennington, J., Sheng, J., Yap, M., Plevka, P., Meng, G., Sun, L., Jiang, W., and Rossmann, M.
909   (2013). Obstruction of dengue virus maturation by Fab fragments of the 2H2 antibody. *J Virol* 87**,** 8909-
910   8915.
911 Wichmann, O., Vannice, K., Asturias, E., De Albuquerque Luna, E., Longini, I., Lopez, A., Smith, P., Tissera, H.,
912   Yoon, I., and Hombach, J. (2017). Live-attenuated tetravalent dengue vaccines: The needs and challenges
913   of post-licensure evaluation of vaccine safety and effectiveness. *Vaccine* 35**,** 5535-5542.
914 World Health Organization (2017). Dengue vaccine: WHO position paper, July 2016 - recommendations. *Vaccine*
915   35**,** 1200-1201.
916 Yang, Y., Meng, Y., Halloran, M., and Longini, I. (2018). Dependency of Vaccine Efficacy on Preexposure and Age:
917   A Closer Look at a Tetravalent Dengue Vaccine. *Clin Infect Dis* 66**,** 178-184.
918 Zhang, S., Tan, H., Hanson, B., and Ooi, E. (2010). A simple method for Alexa Fluor dye labelling of dengue virus.
919   *J Virol Methods* 167**,** 172-177.
920 Zhang, X., Ge, P., Yu, X., Brannan, J., Bi, G., Zhang, Q., Schein, S., and Zhou, Z. (2013a). Cryo-EM structure of
921   the mature dengue virus at 3.5-Å resolution. *Nat Struct Mol Biol* 20**,** 105-110.
922 Zhang, X., Sheng, J., Austin, S., Hoornweg, T., Smit, J., Kuhn, R., Diamond, M., and Rossmann, M. (2015).
923   Structure of acidic pH dengue virus showing the fusogenic glycoprotein trimers. *J Virol* 89**,** 743-750.
924 Zhang, X., Sheng, J., Plevka, P., Kuhn, R., and Diamond, M. (2013b). Dengue structure differs at the temperatures
925   of its human and mosquito hosts. *Proc Natl Acad Sci U S A* 110**,** 6795-6799.

926

927

928

A

1   91 92   166

pr   M

MH MT1 MT2

	P8	P7	P6	P5	P4	P3	P2	P1	P1'	Pitou Score	Relative prM-to-E ratio
DENV serocomplex											
DENV-2	G	E	H	R	R	E	K	R	S	11.01	82.3
DENV-1	G	E	H	R	R	D	K	R	S	6.90	ND
DENV-3	G	E	H	R	R	D	K	R	S	6.87	ND
DENV-4	G	E	R	R	R	E	K	R	S	13.26	53.6
JEV serocomplex											
JEV	R	H	S	K	R	S	R	R	S	14.92	ND
SLEV	G	H	S	R	R	S	R	R	S	14.74	ND
WNV	R	H	S	R	R	S	R	R	S	15.40	43.7
Other serocomplex											
TBEV	Q	E	G	S	R	T	R	R	S	13.65	41
YFV	G	R	S	R	R	S	R	R	A	13.28	38.6
CFAV	V	V	K	K	R	E	K	R	S	7.25	31
Zika	G	E	A	R	R	S	R	R	A	13.82	ND
mD2VLP	V	V	K	K	R	S	K	R	S		13.7
imD2VLP	G	E	H	R	R	E	S	T	S		100

B

imD2VLP mD2VLP

72 —

55 —   E

100 123.8

Blot: MHIAF

imD2VLP mD2VLP

26 —

17 — prM

100 10.7

Blot:2H2

imD2VLP mD2VLP

17 —

10 — M

0 100

Blot: anti-M

929

930   Fig. 1. Comparison of the prM junction cleavage efficiency among different DENV-2 virus-like

931   particles (D2VLPs). (A) Schematic drawing of the prM protein. The C-terminal of the prM protein

932   contains an α-helical domain (MH) in the stem region, followed by two transmembrane domains

933   (MT1 and MT2). Numbers refer to the position of the amino acids in the polyprotein starting at the

934   first amino acid of prM according to DENV-2 (NP_056776). Single letter designations of amino acid

935   sequence alignment of representative strains from different serocomplexes of flaviviruses at the prM

936   junction site includes dengue virus serotypes 1-4 (DENV-1 to DENV-4), Japanese encephalitis virus

937   (JEV), St. Louis encephalitis virus (SLEV), West Nile virus (WNV), tick-borne encephalitis virus

938   (TBEV), yellow fever virus (YFV), cell-fusion agent virus (CFAV), Zika virus (ZKV), immature

939   DENV-2 VLP (imD2VLP) and mature DENV-2 VLP (mD2VLP). Numbers with P in the beginning

940   refer to the positions of the amino acid relative to the prM cleavage site in the proximal direction

941   (without apostrophe) and the distal direction (with apostrophe). Protein sequences were aligned, with

942   the key P1 and P4 positions within the furin cleavage sites highlighted. The arrow indicates the prM

943   cleavage site. The amino acids in red indicate the residues different from DENV-2. The PiTou 2.0

944   furin cleavage prediction scores are shown on the right for each sequence and the higher scores

945   indicate the higher efficiency of furin cleavage. The relative quantity of prM and E of the wild-type

946   and mutant DENV-2 VLP with P1-8 replacement (from other flaviviruses as shown) was measured

947   by ELISA using MAb 3H5 (specific to E domain III of DENV-2) and MAb 155-49 (specific to

948   DENV prM). The relative prM-to-E ratios were calculated by absorbance for prM/absorbance for E

949   protein with reference to imD2VLP, whose pr portion was set as 100% uncleaved, as shown on the

950   right. ND: not determined. Data are presented as means from three representative ELISA

951   experiments with two replicates. (B) Culture supernatants of mD2VLP and imD2VLPs were

952   collected and purified   after electroporation with the respective plasmids. Five micrograms of

953   proteins were loaded onto a 12% non-reducing Tricine-SDS-PAGE. E, prM and M proteins were

43

954   assayed by Western blot using mouse hyper-immune ascitic fluids (MHIAF, 1:2000), MAb 2H2 (0.5

955   µg/mL) and anti-M protein mouse sera (1:25), respectively. E and prM proteins were visualized with

956   enhanced chemiluminesence (ECL); however, M protein was visualized by TMB substrate to avoid

957   high background. The number below each blot shows the relative densitometric quantification of E,

958   prM and M protein bands by Bio-1D software.

959

960

A

160
140
120 (Å)

B

ecto-domain

E-H2
E-H1
E-H3

H-layer

T-layer

lipid
membrane

14.4Å

E-T2 E-T1 M-T2 M-T1 E-T1 E-T2

DENV virion

mD2VLP

H-layer

T-layer

lipid
membrane

12.8Å
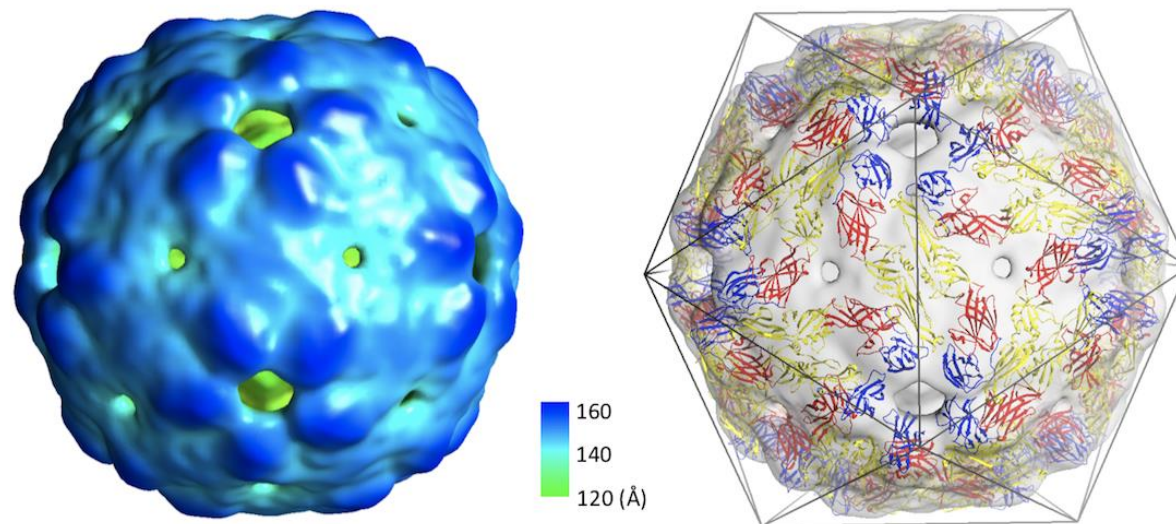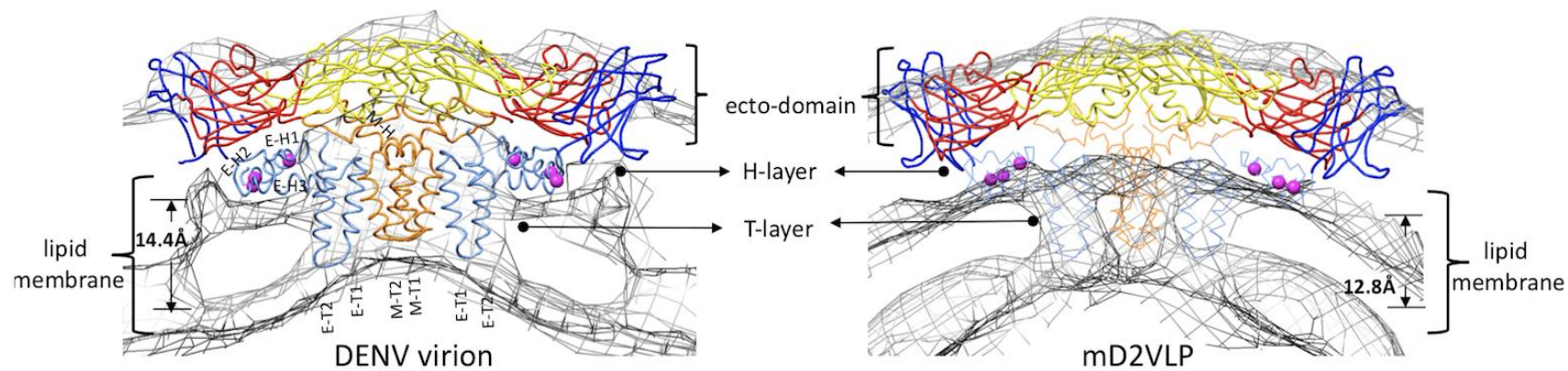
962 **Figure 2. The structure of mature form virus-like particles of dengue virus serotype 2 (mD2VLP). (A)** The reconstructed cryo-

963 EM map of the DENV VLPs (left panel) were presented with the radial color-code indicated (left), the size of the particle is 31nm.

964 Fitting of atomic E, M surface protein (PDB: 3J27) into cryo-EM density map (right) showed that the VLP has 60 copies of E in a T=1

965 arrangement. The density map was shown as a transparent volume rendering into which was fitted the backbone structures of the E

966 ecto-domain. The domains I, II, and III were highlighted in red, yellow and blue, respectively. The cage indicated the icosahedral

967 symmetry. **(B)** The cross section showed the fitted E:M:M:E heterotetramer (PDB: 3J27) into DENV virion (left) and into mD2VLP

968 (right). The map density was in mesh presentation. The atomic model of E:M:M:E heterotetramer was showed in ribbon. Domain

969 definition of dengue E was the same as the previous description, the transmembrane domain of E was colored as light blue, the M

970 protein was in orange color. It was clear that the density of H-layer which is composed of E-H1 to E-H3 and M-H was more solid

971 while the density in T-layer which contains E-T1, E-T2, M-T1 and M-T2 was weak in VLP than in virion. The residues at 398, 401

972 and 412 in E-H1 of JEV sequence which were proved to play important role in promoting extracellular secretion[28] were shown as

973 magenta spheres. The transmembrane, perimembrane helices and lipid bilayer were labelled, the critical measurements were also

974 shown.

975
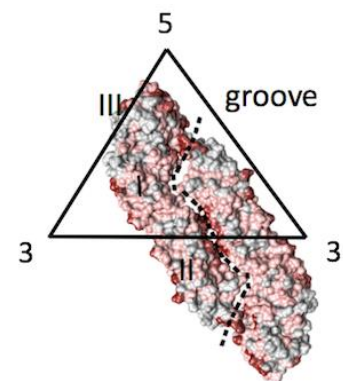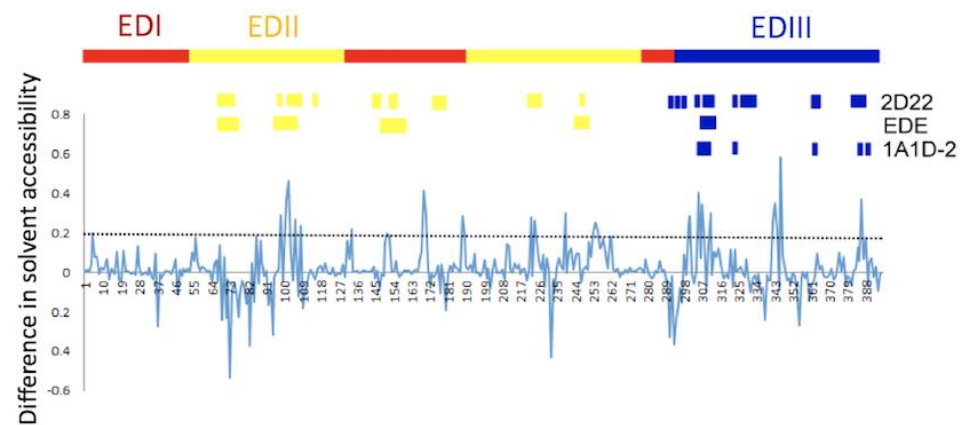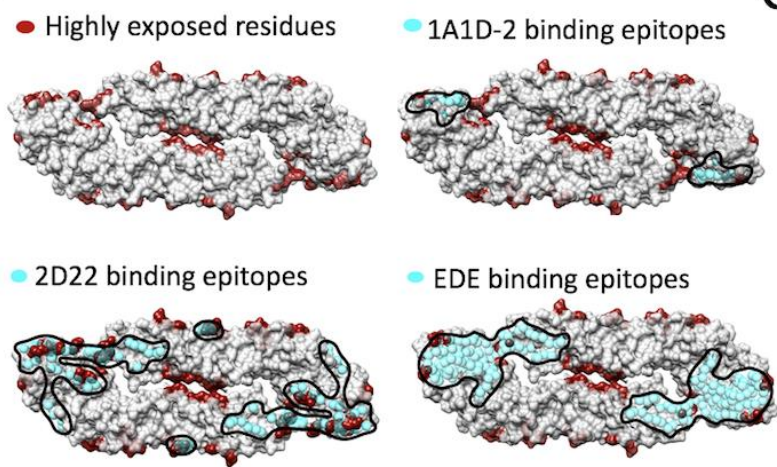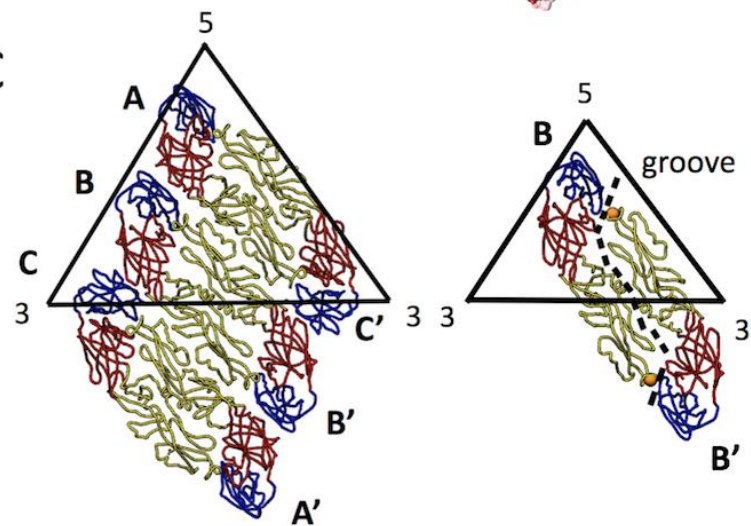
Figure 3. Solvent accessibility of dengue virus serotype 2 virus soluble envelope (sE) protein (A, left) The plot of difference in relative solvent-accessible surface area (Δ%SASA). A positive value of %SASA meant the residue became more exposed when the particle assembly shifts from virion (3 copies of E dimers per icosahedral asymmetric unit) to VLP (1 copy of E dimers per icosahedral asymmetric unit). The black dash line indicated the Δ%SASA ≥0.2 which was defined as highly exposed residues in VLP comparing to virion. The high positive values which were focused in the peptide regions such as the fusion loop peptide (including amino acid (aa) residues ranging from 100-110), aa 169-170 at domain I, aa 222-226, aa 239 and aa 251-262 at domain II as well as A strand of domain III (aa 300-308), the cd loop of domain III (aa 342-348) and G strand (aa 386-388) around the 5-fold openings. The residues interacting with MAb 1A1D-2[30], including residues 305-312, 352, 364, 388 and 390; the residues interacting with MAb 2D22[31], including residues 67-72, 99, 101-104, 113, 177-180, 225-227, 247, 328, 384-386 (Heavy chain); 148-149, 153-155, 291-293, 295, 298, 299, 307, 309-310, 325, 327, 362-363 (light chain) and the residues interacting with human MAb EDE antibodies[19], including aa residues 67-74, 97-106, 148-159, 246-249 and 307-314 were indicated. **(A, right)** The high positive peaks (Δ%SASA ≥0.2), low positive peaks (Δ%SASA between 0 and 0.2) and negative peaks (Δ%SASA ≤0) in the plot were colored by dark red, deem red and grey in the E dimer surface rendering. The groove located within E-dimer interface was outlined. **(B)** The highly exposed residues (Δ%SASA ≥0.2) which were colored by dark red were shown in the surface rendered E-dimer. The residues in E interacting with MAb 1A1D-2, 2D22 and EDE were in cyan spheres showing that they were highly exposed on the m2DVLP surface. Importantly, the binding footprints of the three antibodies were highly overlapping with footprint of highly exposed residues in

993   m2DVLP, and formed a neutralization sensitive patch on m2DVLPs. The areas of the interacting epitopes are circled by black lines.

994   **(C)** The E protein forming the rafts in virion were shown in the left panel where the three individual E proteins in the asymmetric unit

995   are labeled A, B, and C of the E proteins, in the neighboring asymmetric unit are labeled A', B', and C'. The icosahedral 2-fold E

996   protein dimers (B and B') in m2DVLP have moved apart from each other causing the groove (right). The aa 101 which was

997   responsible for DM25-3 antibody binding were shown in orange spheres.

998

999
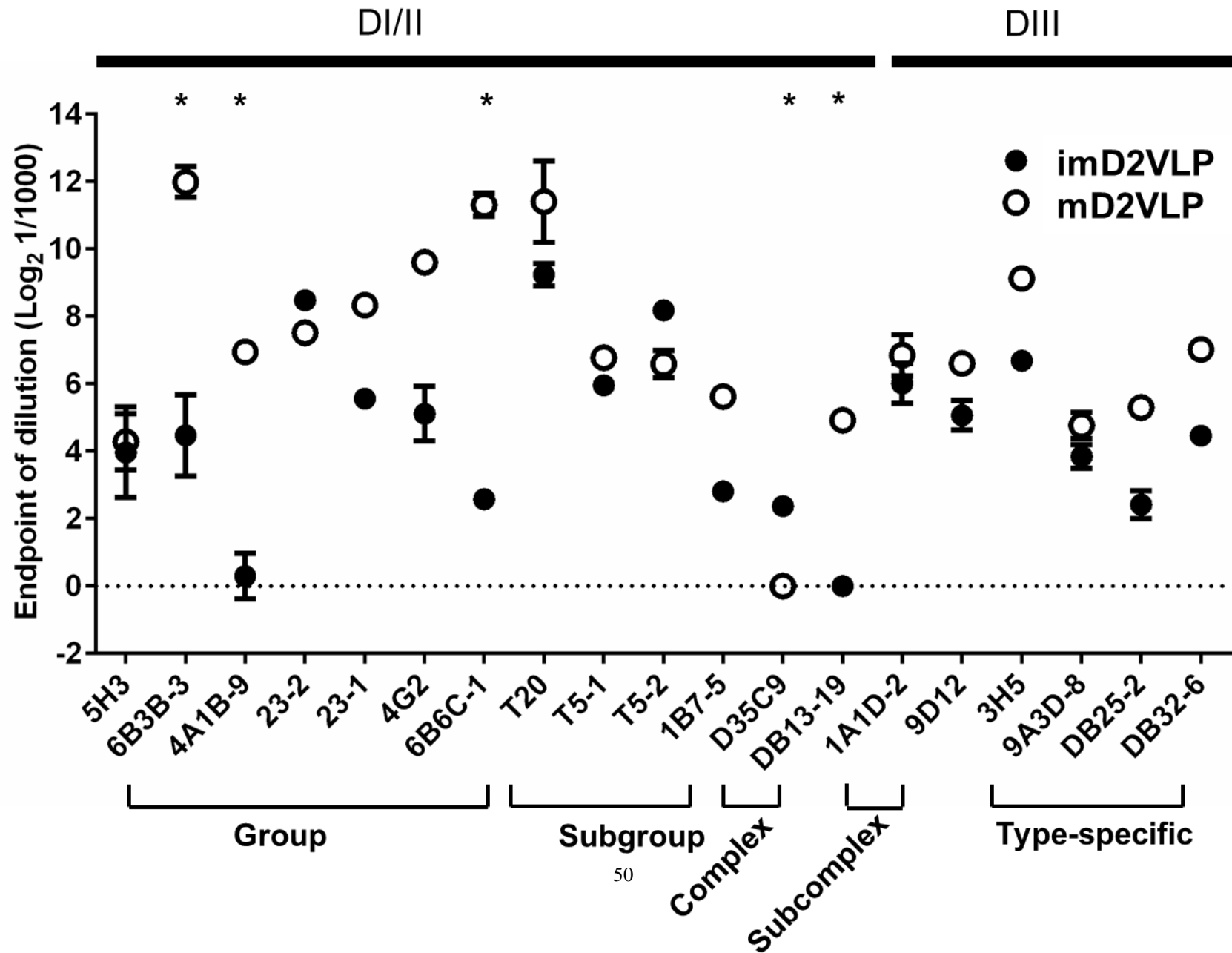
1001   **Fig 4. Summary of binding activity of a panel of anti-E monoclonal antibodies (Mabs) to mD2VLP and imD2VLP. The binding activity of each Mab to**

1002   **two types D2VLP was expressed as means of endpoint dilution with standard deviations from duplicates of representative experiments of three. The**

1003   **dash line represents the minimum dilution of Mab used in the experiment. The asterisk symbol represents statistical significance between mD2VLP**

1004   **and imD2VLP in antibody dilution reaching endpoint with p-value <0.05**

1005

1006

1007

52
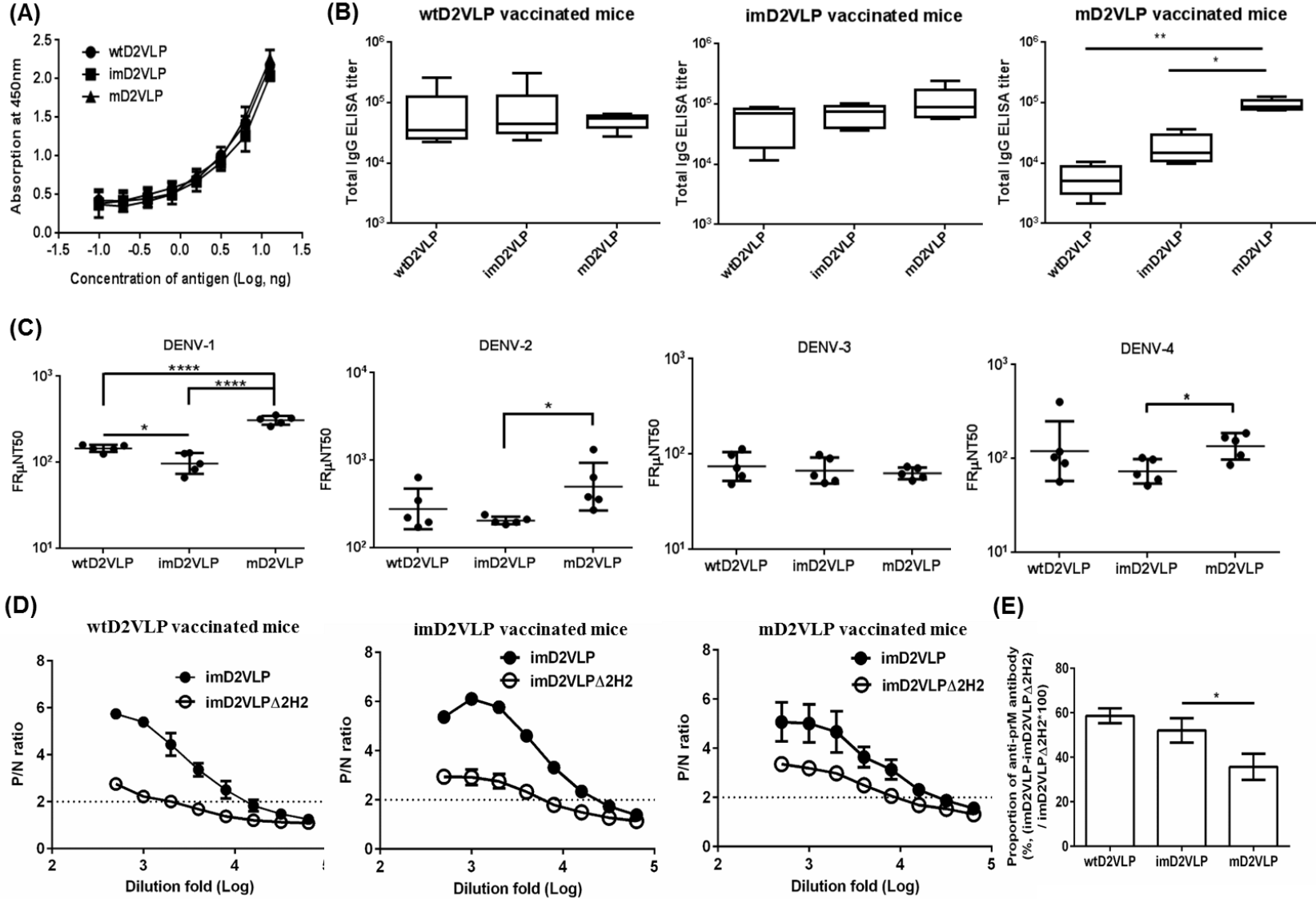
Figure 5. Total antigen-specific IgG, neutralizing titers and proportion of anti-prM antibodies compared among three **groups of mice immunized with wtD2VLP, imD2VLP or mD2VLP. (A)** D2VLPs were concentrated and purified from clarified supernatants. The total protein concentration of purified imD2VLP and mD2VLP were first determined by the Bradford assay and then subjected to antigen-capture ELISA using 2-fold serial dilutions. The standard curve was used to titrate both antigens as equal amounts for the subsequent assays. **(B)** The endpoint IgG titer of 12-week post-immunization mouse sera was measured by antigen-capture ELISA, using equal amounts of homologous and heterologous purified D2VLP antigens. All endpoint titers were $\log_{10}$ transformed and depicted as geometric means with 95% confidence intervals. **(C)** The neutralizing antibody titers at 50% antigen focus-reduction micro neutralization (FRµNT50) in Vero cells infected with DENV-1 to 4. **(D)** Binding reactivity of serial dilutions of anti-wtD2VLP (left), anti-imD2VLP (center), and anti-mD2VLP (right) mouse sera were analyzed by ELISA using equal amounts of wild-type (imD2VLP) and mutant imD2VLP (Δ2H2) antigens. **(E)** Proportions of 2H2-like, anti-prM antibodies from two different D2VLP immunization groups were calculated based on the formula 100*[(OD450imD2VLP-OD450Δ2H2)/OD450imD2VLP] at a 1:1000 dilution of mouse sera. All data presented are based on a representative of three independent experiments with two replicates from n=5 mice sera per group per experiment and expressed as mean $\pm$ SEM. The statistical significance was determined using the two-tailed Mann-Whitney *U* test to account for non-normality of the transformed data. *, $P < 0.05$; **, $P < 0.01$; ****, $P < 0.0001$.

1023
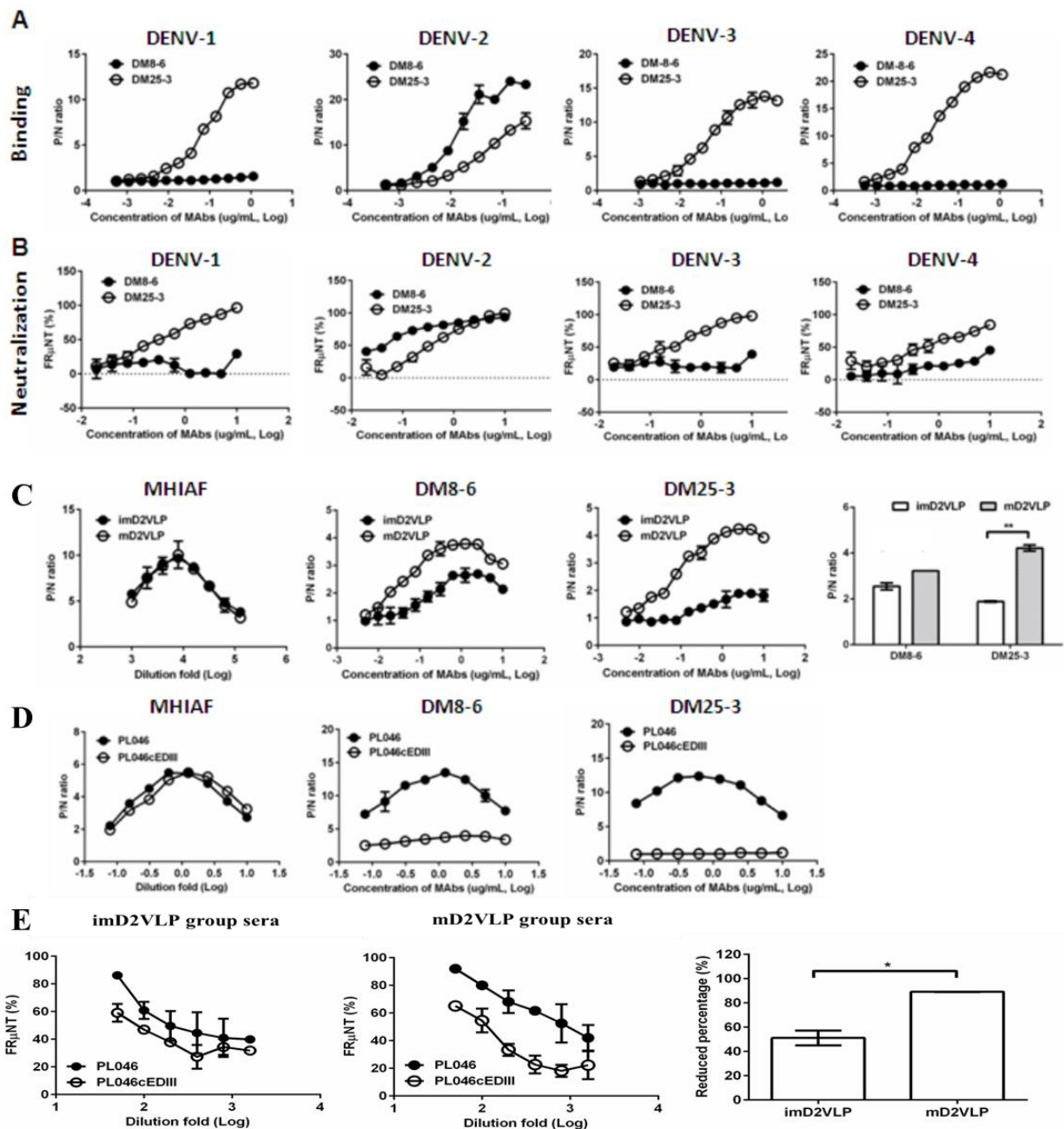
Figure 6. Characterization of murine monoclonal antibodies (MAbs) generated from mouse

splenocytes following immunization with mD2VLP. Binding (A) and neutralizing (B)

activities of MAbs DM8-6 and DM25-3 against DENV-1 to 4 were measured by ELISA and the

focus-reduction micro-neutralization test (FRμNT). (C) Binding curves of MAb DM8-6 (center

left) and DM25-3 (center right) against imD2VLP and mD2VLP were performed using ELISAs.

1029   Equal amount of both imD2VLP and mD2VLP was properly titrated by antigen-capture ELISA

1030   using mouse hyper-immune ascitic fluid (MHIAF) against DENV-2 (left). The difference in

1031   binding activities of both MAbs is presented by a bar graph (right). **(D)** A recombinant DENV-2

1032   virus was produced by replacing domain III with a consensus sequence of domain III

1033   (PL046cEDIII)[31] and the binding activity of DM8-6 (center) and DM25-3 (right) was compared

1034   with that of parental DENV-2 strain PL046. Equal amount of both PL046 and PL046cEDIII was

1035   properly titrated by antigen-capture ELISA using mouse hyper-immune ascitic fluid (MHIAF)

1036   against DENV-2 (left). **(E)** FRμNT of two-fold diluted mice sera immunized with mD2VLP and

1037   imD2VLP against parental PL046 and PL046cEDIII DENV-2 viruses (n=5 per group per

1038   experiment). The differences in FRμNT50 from mD2VLP and imD2VLP immunization groups

1039   were converted to bar chart at 1:1000 fold dilution of mice sera. The conversion was based on

1040   the formula 100*[FRμNT50 of (PL046- PL046cEDIII)/ FRμNT50 of PL046]. P/N ratio refer to

1041   the antibody binding magnitude between designated VLP-containing (P) and VLP-free culture

1042   supernatant (N) by dividing the absorbance of P by that of N. The data are presented as means $\pm$

1043   SEM from three independent experiments with two replicates. The two-tailed Mann-Whitney *U*

1044   test was used to test statistical significance. *, *P* <0.05. **, *P* <0.01.

1045

1046

55

1047
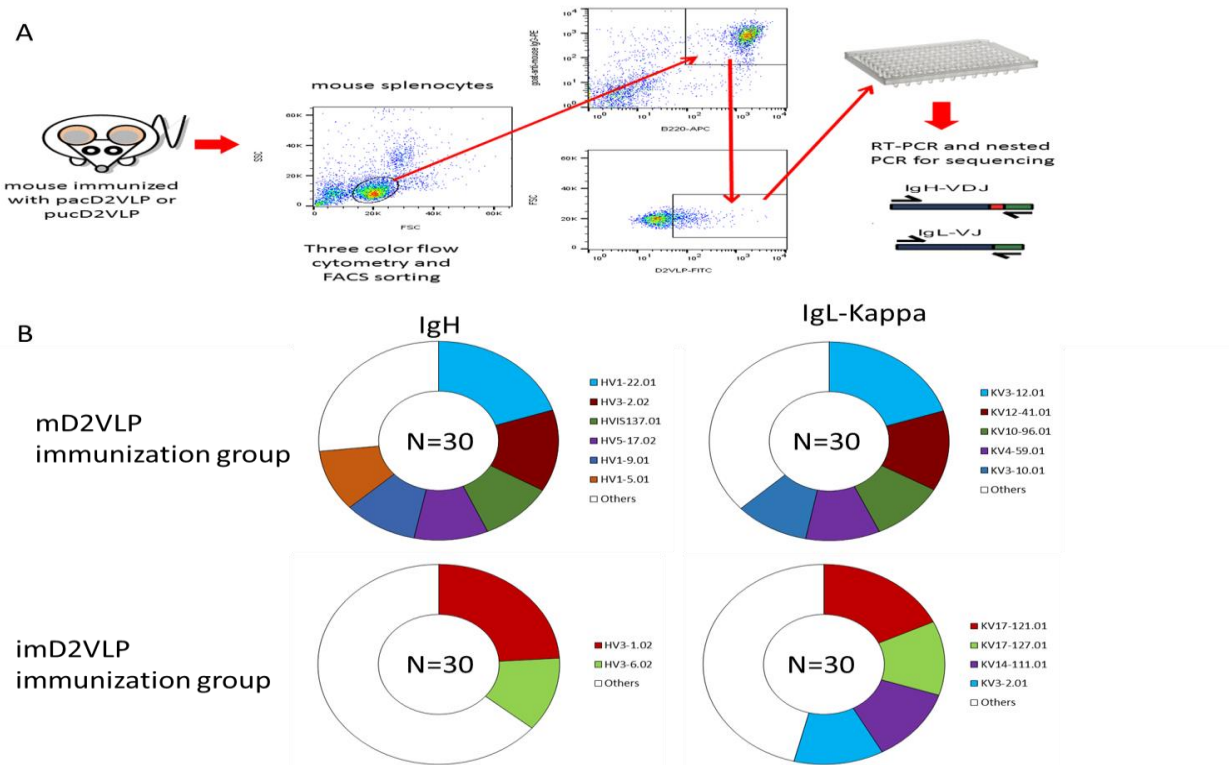
Figure 7. Overview of the experimental design and DENV-specific B-cell repertoires from the splenocytes obtained from mD2VLP- and imD2VLP-immunized mice. (A) Single DENV(+), B220(+) and IgG1(+)-specific B cell from the spleen of vaccinated mice was sorted into 96-well plates by FACS. The IgH and IgL gene transcripts of each single B cell were amplified by RT-PCR and nested PCR using gene-specific primers. **(B)** B-cell producing heavy chains and light chains encoded by the same IgH and IgL gene loci were grouped by the same color. The proportions of IgH- or IgL (κ-chain only)-genes are indicated by various colors corresponding to frequencies of the B-cell population of each vaccinated group. Frequencies greater than 10% are shown in various colors, otherwise they are grouped together and shown in white.

1058

56
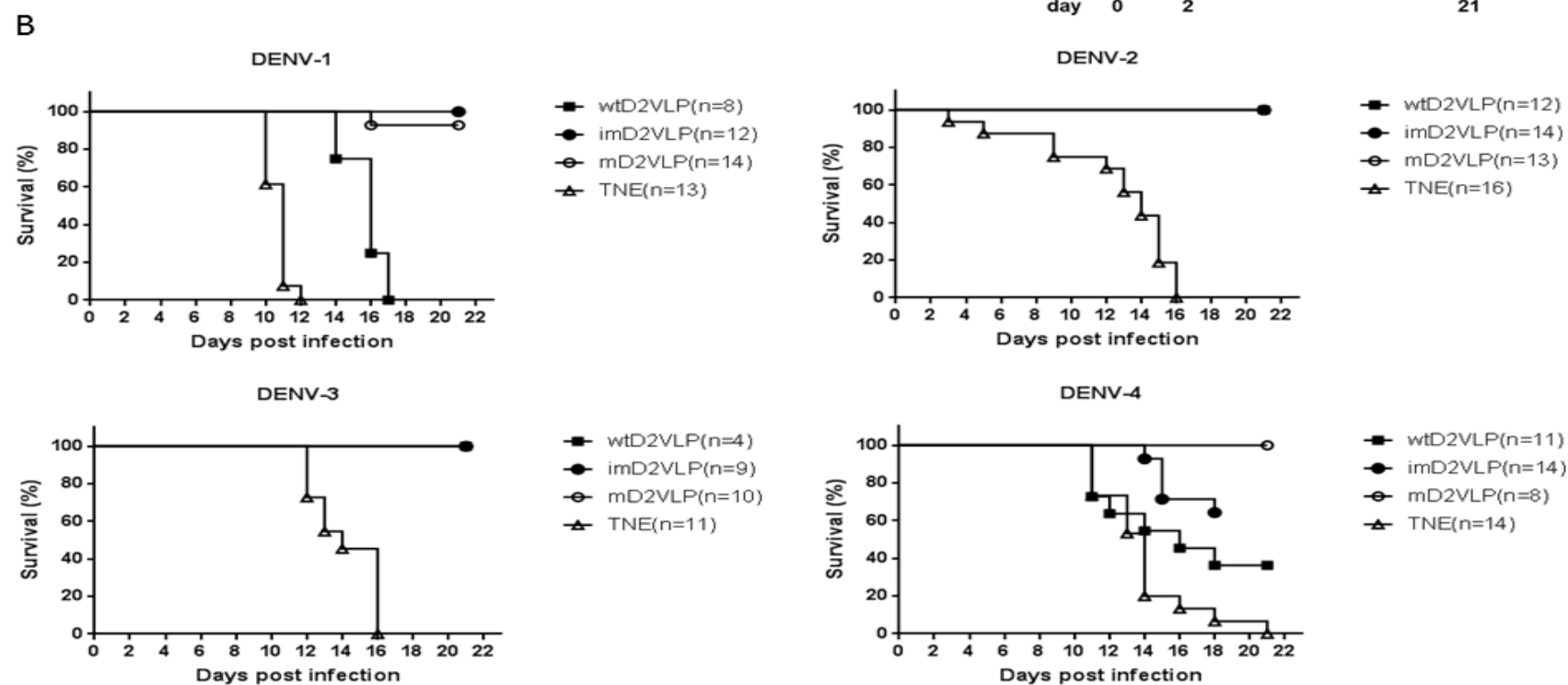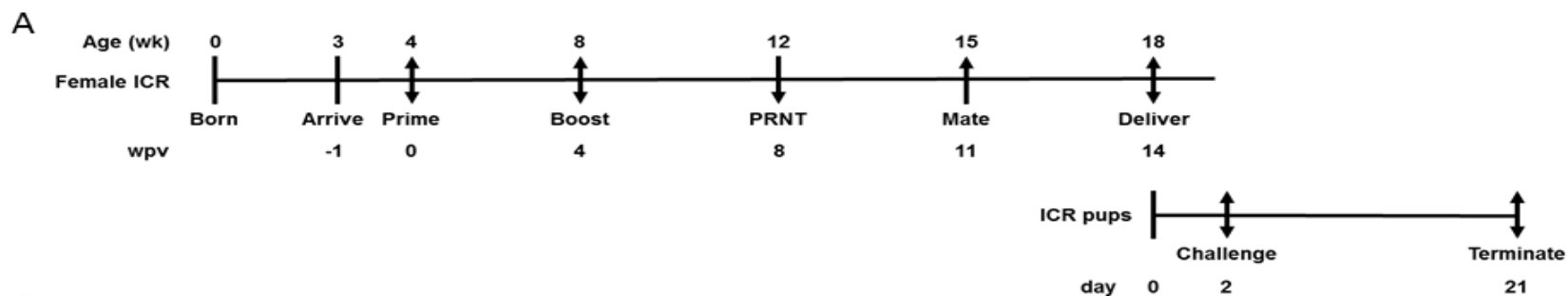
Figure 8. Schematic presentation of the schedule and survival curves for mouse immunization and challenge. **(A)** Groups of four 4-week-old, female, ICR mice were injected intramuscularly with imD2VLP and mD2VLP at week post vaccination (wpv) 0 and 4 at a dose of 4 μg/100 μL. Mice were bled from the retro-orbital sinus at week 4 following the second injection, and individual mouse serum collected from immunized females 1 week prior to mating was evaluated for the presence of the total IgG titer and the virus neutralization response by ELISA and focus-forming micro-neutralizing assay (FRNT). For the evaluation of passive protection by maternal antibody, ICR pups from the mating of non-immunized males with immunized females 11 weeks post initial vaccination were obtained for viral challenge. Pups from unvaccinated females were used as the challenge control. ICR pups from the designated groups were challenged individually through intracranial route at 2 days after birth with 10^4 focus-forming unit (FFU) which were equivalent 141, 61, 11, 1000 times of 50% lethal doses (LD50) of DENV-1, to DENV-4, respectively. The percent survival of the mice was evaluated daily for up to 21 days. **(B)** Survival curve of pups delivered from the female mice receiving mD2VLP, imD2VLP monovalent vaccine or TNE control, then challenge with DENV-1 to 4 after birth. The in vivo protective efficacy of DENV-2 monovalent vaccine is maturity-dependent. N in parentheses indicated the numbers of pups of each group. Kaplan-Meier survival curves were analyzed by the log-rank test. ***, $P < 0.001$.

2

Supplementary Materials

Table S1. Nucleotide sequences of primers for site-directed mutagenesis used in this study

Name	Primer sequence (5'-3')	Amino acid substitution	Secreted
mD2VLP	ACGTGTACCACCATGGGAGAA**AAAAAA**AGAGAAAAAGATCAGTG	His-Lys, Arg-Lys	Y
	TGGGACGTGTACCACCATG**GTAGTA**AAAAAAAGAGAAAAAGATC	Gly-Val, Glu-Val	Y
	CATGGTAGTAAAAAAAAGA**TCA**AAAAGATCAGTGGCACTCG	Glu-Ser	Y
imD2VLP	AGAACATAGAAGAGAA**TCAACA**TCAGTGGCACTCG	Lys-Ser, Arg-Thr	Y
△2H2	AGGGAAAAGTCTTCTGTTT**CCA**ACAGAGGATGGCGTGAAC	Lys-Pro	Y
	CAGCAGACAAGAGAAAGGG**GAC**AGTCTTCTGTTTCCAACAG	Lys-Asp	Y
	CATAGCTTGTGCAGGCGCC**GCC**CATTTAACCACACGTAAC	Phe-Ala	Y
W101G	TCCATGGTAGACAGAGGA**GGG**GGAAATGGATGTGGACTA	Trp-Gly	Y
N103K	GACAGAGGATGGGGA<u>AAA</u>GGATGTGGACTATTTGGA	Asn-Lys	N
G104Q	AGACAGAGGATGGGGAAAT<u>CAA</u>TGTGGACTATTTGGAAAGG	Gly-Gln	N
K307E	TCTATGTGCACAGGAAAGTTT**GAA**GTTGTGAAGGAAATAGCAGAA	Lys-Glu	N
K310E	ACAGGAAAGTTTAAAGTTGTG**GAG**GAAATAGCAGAAACAC	Lys-Glu	Y
E311R	CAGGAAAGTTTAAAGTTGTGAAG**CGA**ATAGCAGAAACACAACATGG	Glu-Arg	Y
E314R	AAAGTTGTGAAGGAAATAGCA**CGA**ACACAACATGGAACAATAGTT	Glu-Arg	N
T315H	TTGTGAAGGAAATAGCAGAA**CAC**CAACATGGAACAATAGTTAT	Thr-His	N
Q316P	GTGAAGGAAATAGCAGAAACA**CCA**CATGGAACAATAGTTATCAGA	Gln-Pro	Y
H317E	AAGGAAATAGCAGAAACACAA**GAA**GGAACAATAGTTATCAGAGTG	His-Glu	Y
P364R	GACAGAAAAAGATAGC**CGG**GTCAACATAGAAGCAGAACCT	Pro-Arg	N

3

| W391G | GGACAACTGAAGCTCAAC**GGG**TTTAAGAAAGGAAGCAC | Trp-Gly | N |
| F392A | ACAACTGAAGCTCAACTGG**GCT**AAGAAAGGAAGCACGCTG | Phe-Ala | Y |

1076

1077

4

| F392A | ACAACTGAAGCTCAACTGG**GCT**AAGAAAGGAAGCACGCTG | Phe-Ala | Y |

1078

1079

5

(A)

imD2VLP wtD2VLP mD2VLP

E

PrM

M

(B)

Percentage of pr peptide on particles (%, imD2VLP as 100%)

imD2VLP   wtD2VLP   mD2VLP
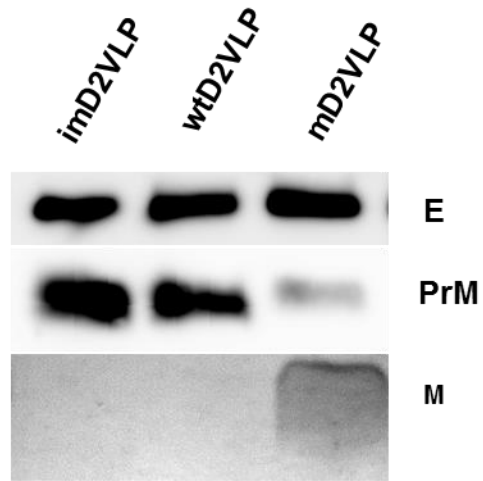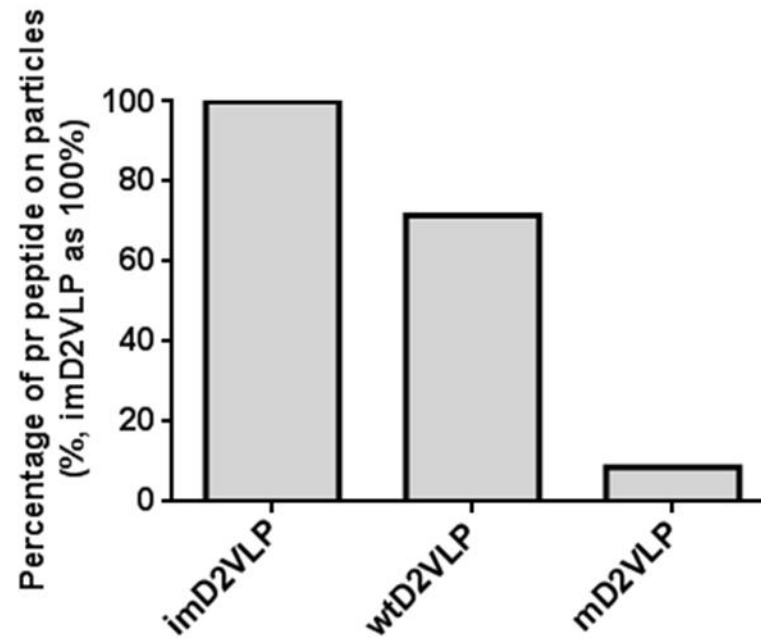
1080

1081

Figure S1. Comparison of prM cleavage among different DENV-2 virus-like particles (D2VLP). (A) Culture supernatants of mD2VLP and imD2VLPs were collected and purified after electroporation with the respective plasmids. Five micrograms of proteins were loaded onto a 12% non-reducing Tricine-SDS-PAGE. E, prM and M proteins were assayed by Western blot using mouse hyper-immune ascitic fluids (MHIAF, 1:2000), MAb 2H2 (0.5 µg/mL) and anti-M protein

6

1085   mouse sera (1:25), respectively. E and prM proteins were visualized with enhanced chemiluminesence (ECL); however, M protein was visualized by TMB

1086   substrate to avoid high background. (B) Percentages of pr-peptide remaining on particles were measured by calculating the relative densitometric quantity of

1087   prM band by Bio-1D software.

1088

(A)

wtD2VLP

imD2VLP

mD2VLP

(B)

(C)
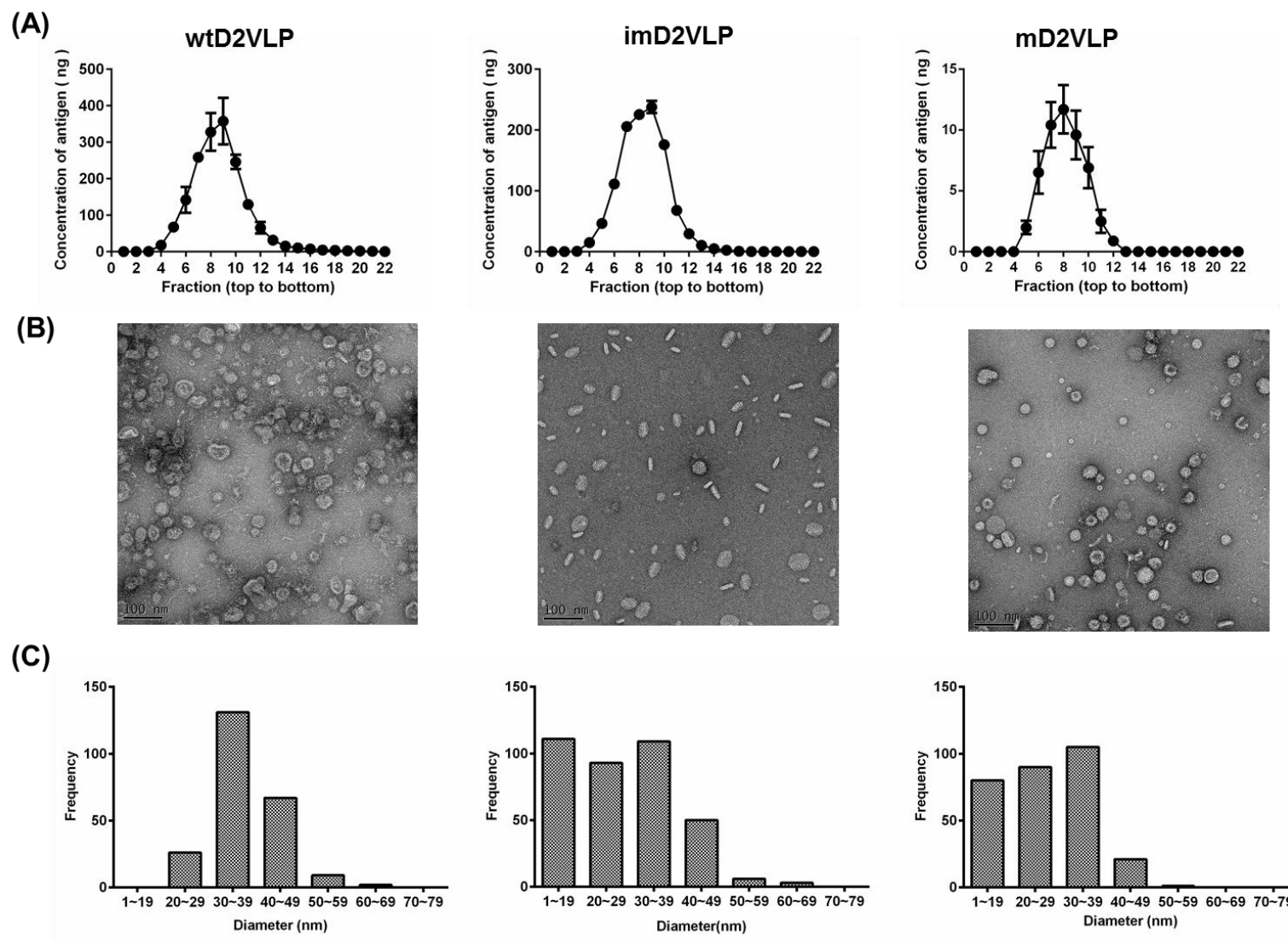
1090
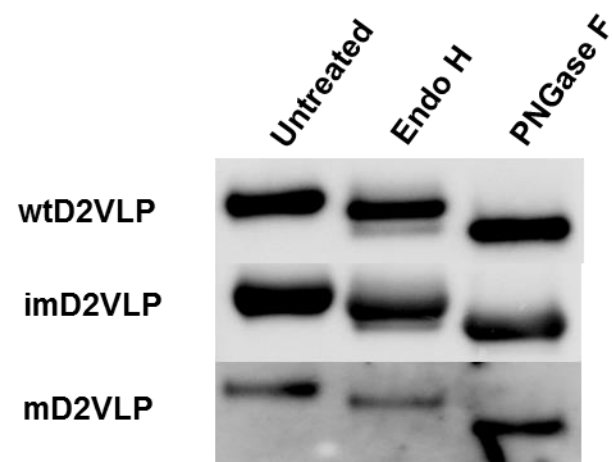
1091

1092

1093   Figure S2. Comparison of physical properties of D2VLP among different DENV-2 virus-like particles (D2VLP). (A) Equilibrium banding profiles

1094   of wtD2VLP (left), imD2VLP (center) and mD2VLP (right) after rate-zonal centrifugation on a 5-25% linear sucrose density gradient at

1095   25,000 rpm for 3 hours. Equivalent amounts (50μl) of D2VLP from each fraction were subjected to antigen-capture ELISA. (B) Electron

1096   micrographs at 50,000-fold magnification of wtD2VLP (left), imD2VLP (center) and mD2VLP (right) stained with uranyl acetate from the

1097   peak fraction in (A). (C) The diameter of 200 randomly selected particles of wtD2VLP (left), imD2VLP (center) and mD2VLP (right) from

1098   representative electron micrographs as in (B) were determined by software Gatan Digital Micrograph. (D) Endoglycosidase treatment of

9

1099   purified wtD2VLP, imD2VLP and mD2VLP. Samples were treated with PNGase F or Endo H and compared with untreated controls by

1100   10% non-denaturing SDS-PAGE and immunoblotting with DENV-2 mouse hyper-immune ascitic fluid (MHIAF).

1101

1102
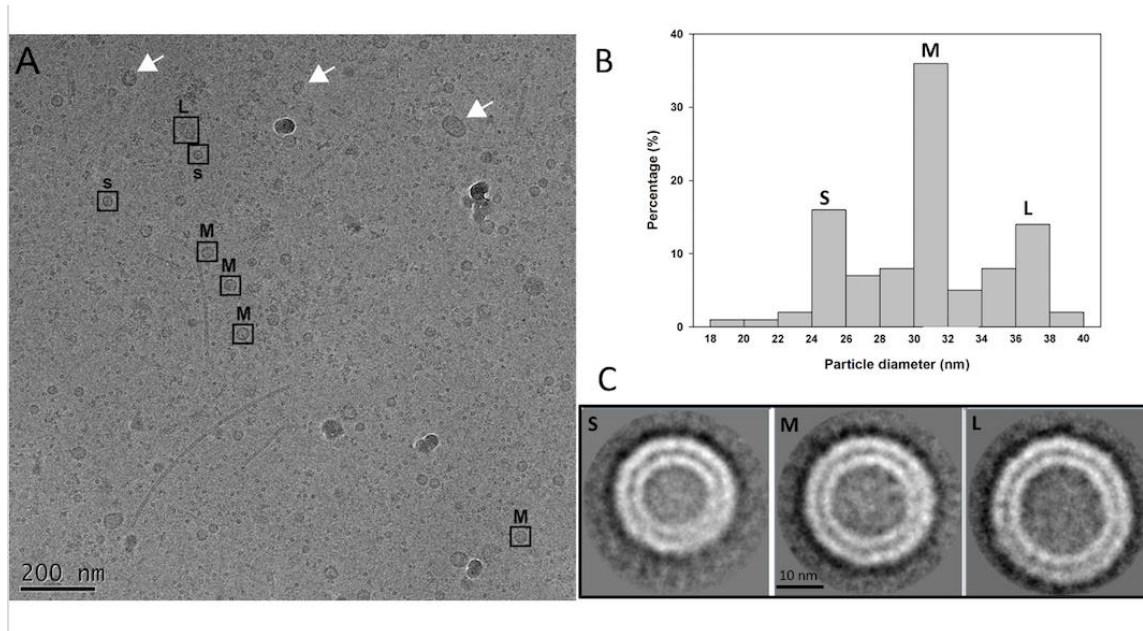
Figure S3. The cryo-EM images and 2D analysis of the particles. (A) Cryo-EM images of purified mD2VLP showed spherical particles (boxed) among irregular or incomplete structures (arrows). Irregularly-shaped particles were eliminated through visual inspection, while the spherical particles were subjected to further image analyses. (B) The particle size analyses showed the size variation in the sample and that the major peaks were located at ~26nm, ~31nm and ~36nm diameter size classes which were therefore denoted by small ('S'), medium ('M') and large ('L'). Each of the 'S', 'M' and 'L' particles identified was labeled. (C) The 2D image analyses showed that the particles had two distinct layers and that the particles classes with diameters of ~31nm had more solid features than others.

11
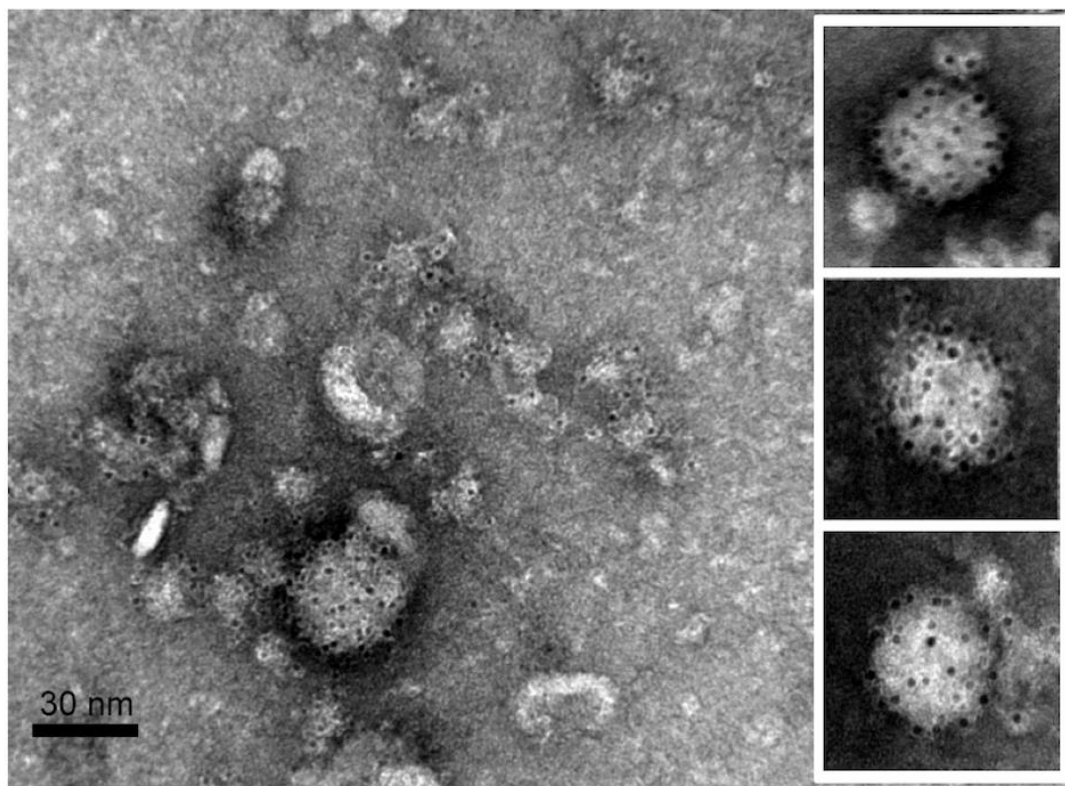
1111

Figure S4. The EM images of immunogold-labeled mD2VLPs. The E proteins were labeled with domain III-specific monoclonal antibody (MAb 32-6), and

conjugated with 6-nm gold particles.

1114

1115

1116

1117

1118
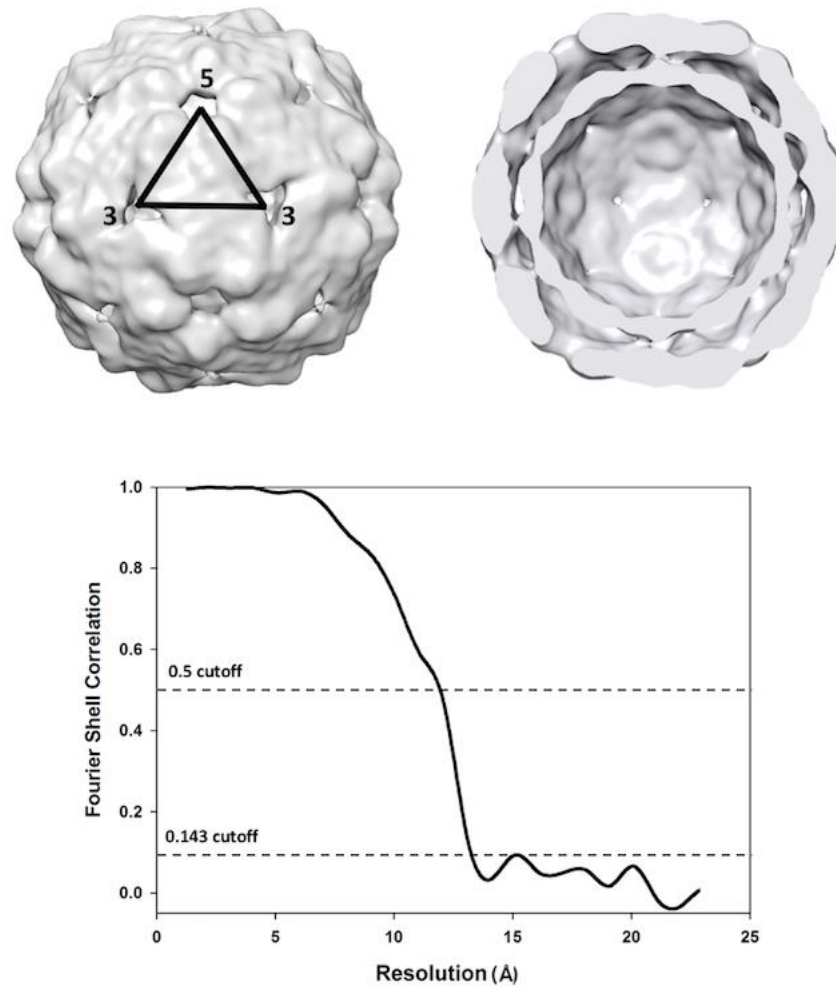
Figure S5. The cryo-EM structure of m2DVLP. The reconstructed cryo-EM map of the mD2VLPs was shown on the left. An asymmetric unit was indicated. On the right, the closest half of the density map has been removed to reveal the hollow structure. The resolution of the final reconstruction was determined to be 13.1Å using a gold standard resolution estimate at cutoff 0.143 (lower panel).

1

1124

1125

1126
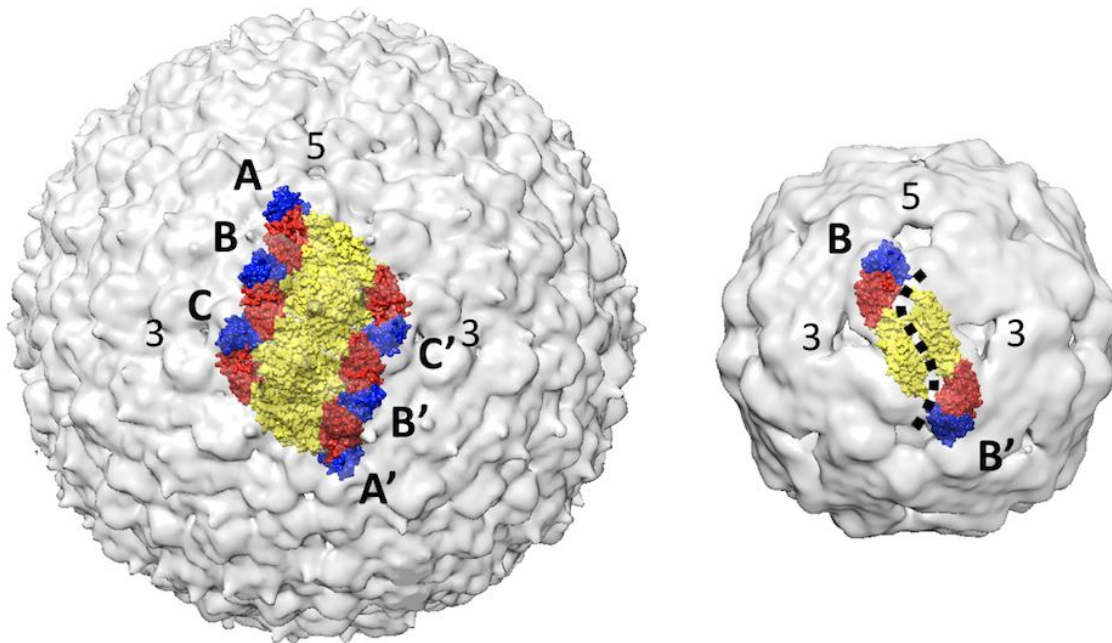
1127   Figure S6. The E protein rafts in a virion (left) and mD2VLP (right). The E protein forming

1128   the rafts in the virion were shown in the left panel where the three individual E proteins in the

1129   asymmetric unit were labeled A, B, and C and the E proteins in the neighboring asymmetric

1130   unit are labeled A', B', and C'. The icosahedral 2-fold E protein dimers (B and B') of

1131   mD2VLP moved apart from each other causing the groove (dashed line, right).

1132

1133

1134

2

1135

1136

1137
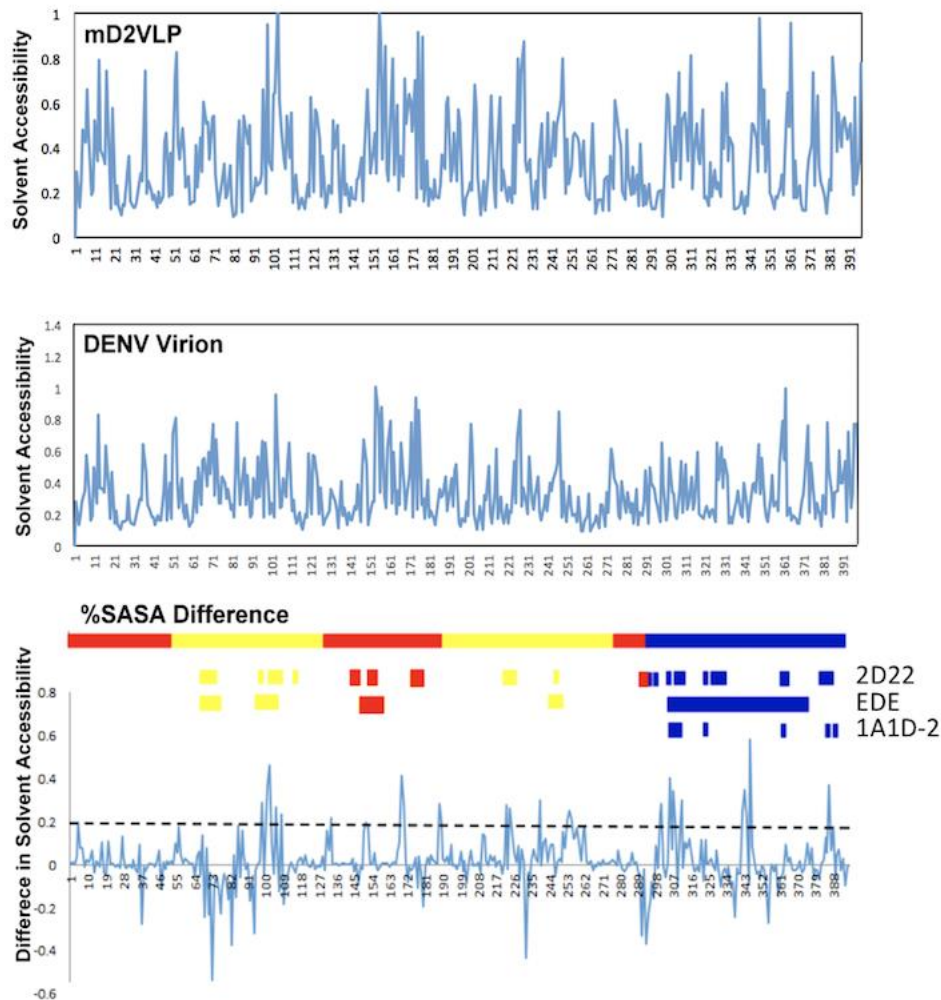
Figure S7. The solvent accessibility analyses. Solvent accessibility of the dengue particle soluble envelope (sE) protein amino acid (aa) residues 1-396 in DENV virion and mD2VLP (middle and top, respectively). The all-atom model of VLP was built using MODELLER[18], and the all-atom model virion was built based on the cryo-EM structure of the mature dengue virus at 3.5Å resolution (PDB ID: 3J27). The relative solvent-accessible surface area (SASA) of both models was calculated using the POPS program. The plot shown represents the

1144   difference in relative solvent-accessible surface area (Δ%SASA) (Bottom). A positive value

1145   of %SASA means the residue becomes more exposed in mD2VLP than in DENV VLP.

1146   Domains I, II and III are highlighted in red, yellow and blue, respectively. The residues

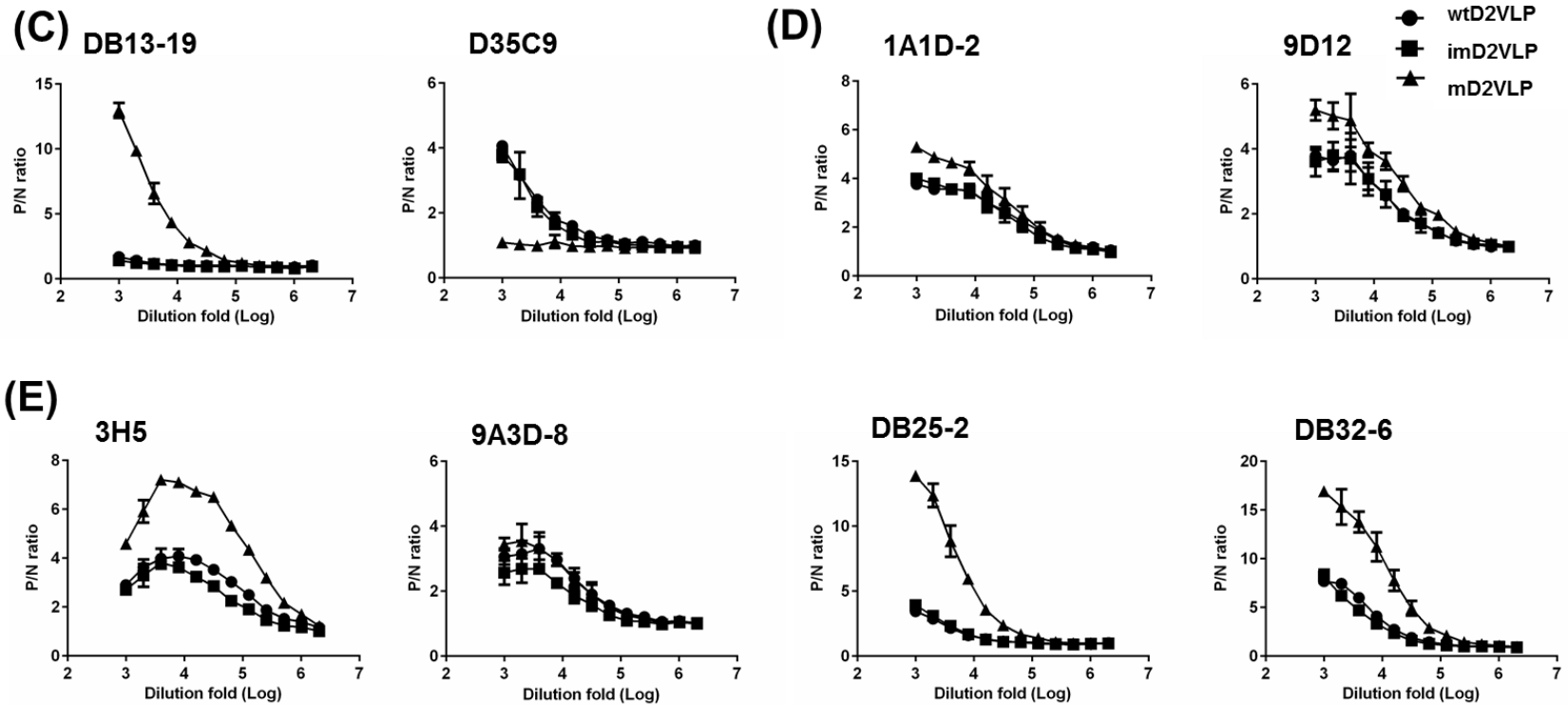1147   interacting with antibodies 2D22, EDE and 1A1D-2 are shown.

1148

1149

(A)

4A1B-9   **6B6C-1**   **6B3B-3**   **23-1**

23-2   **4G2**   **5H3**   **DB42-3**

(B)

T20-1   **T5-1**   **T5-2**   **1B7-5**

Legend: wtD2VLP (●), imD2VLP (■), mD2VLP (▲)

Axes: P/N ratio (y-axis), Dilution fold (Log) (x-axis)

(C) DB13-19, D35C9 **(D)** 1A1D-2, 9D12

(E) 3H5, 9A3D-8, DB25-2, DB32-6

1151

1152
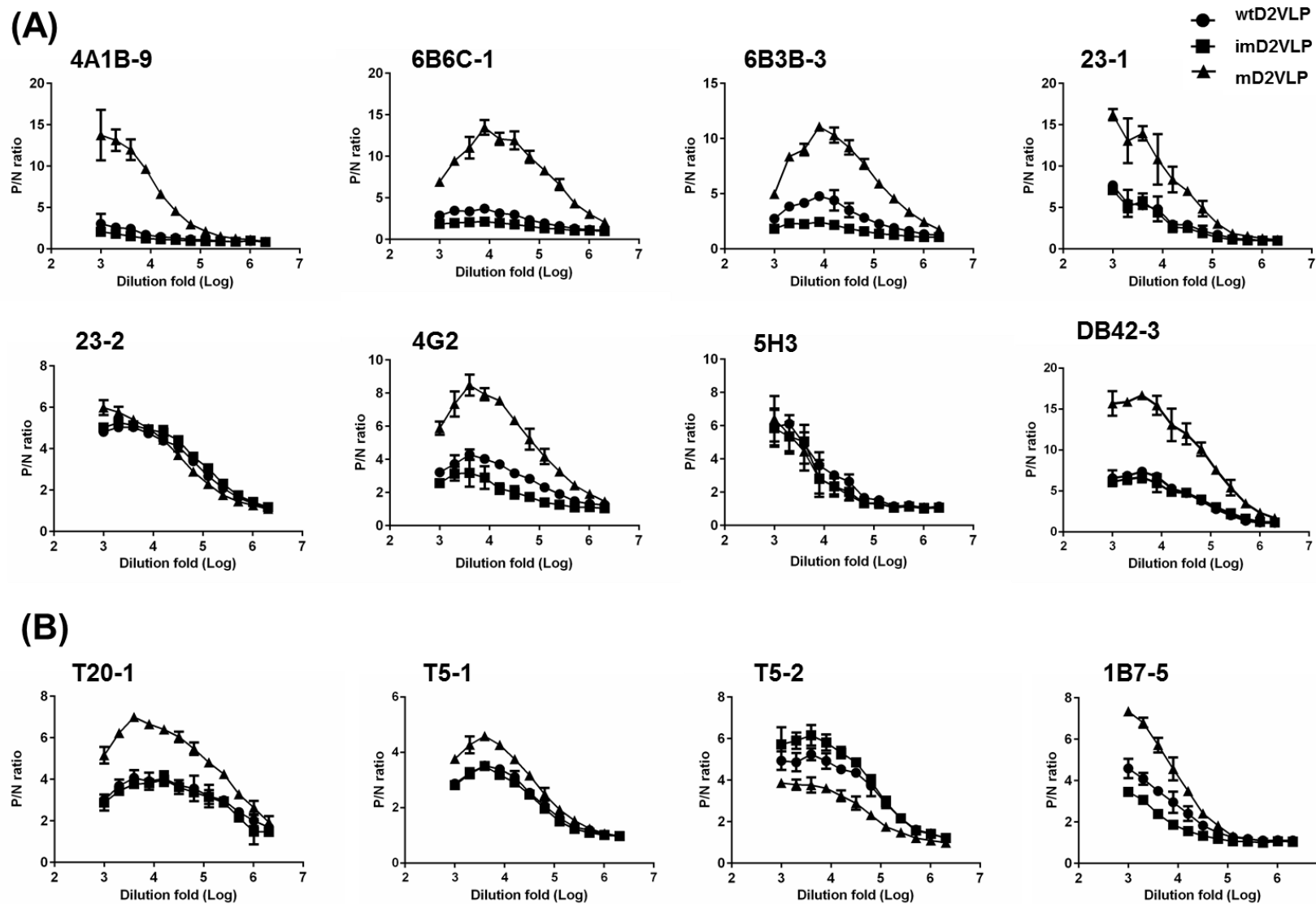
1153 Fig S8. Binding activity curves of a panel of anti-E monoclonal antibodies (Mabs) to three types of D2VLP with different percentage of pr-peptide on particle

1154 surface. Binding curves for (A) eight group-reactive Mabs, (B) four subgroup-reactive Mabs, (C, D) four complex- or sub-complex-reactive Mabs, (E) four

1155 serotype-specific-reactive Mabs were determined by antigen-capture ELISA. Equal quantity of three types D2VLP were first titrated against purified D2VLP

1156 before adding to the wells. Mabs were serially 2-fold diluted starting from 1:1000 dilution. Data are expressed as P/N value by dividing the OD450 value from

1157 each dilution of Mab by the OD450 value from the control COS-1 culture supernatant. Data are means+SEM of duplicates from three representative experiments

1158

1159

1160

1161
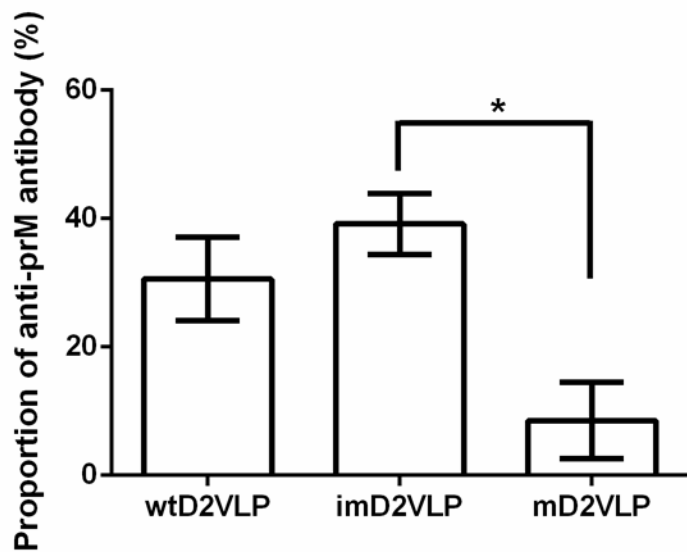
1162 Fig S9. Proportions of anti-prM antibodies from both D2VLP immunization groups were measured using an epitope-blocking ELISA. Percent blocking of HRP-

1163 labeled anti-prM MAb (2H2-HRP) by sera from mice vaccinated with imD2VLP or mD2VLP was determined by the formula 100*[(OD450imD2VLP-

1164 OD450imD2VLP blocked by MAb 2H2)/OD450imD2VLP] using a 1:1000 dilution of mouse sera.

1165

1166

1167

Mab 2H2   Mab 155-49
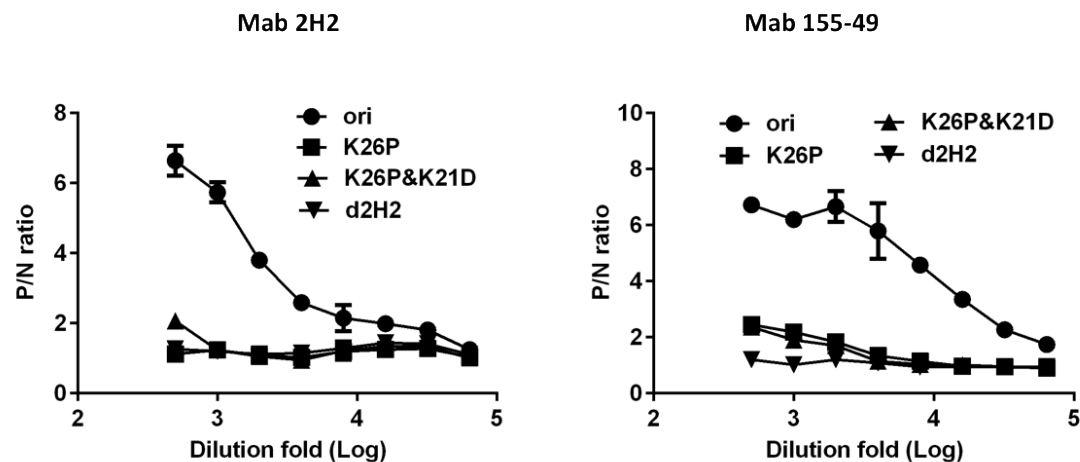
1168

Figure S10. Epitope identification of MAbs 2H2 and 155-49. Single (K26P), double (K26P&K21D) and triple (K26P&K21D&F1A)

mutations were performed on imD2VLP-expression plasmids by site-directed mutagenesis. Various D2VLP mutants were expressed in

COS-1 cells by electroporation with plasmid DNAs as indicated and tissue culture media were clarified 3 days after transfection for antigen-

capture ELISA. Substitutions of K26P on imD2VLP led to a significantly reduced binding activity of MAb 2H2; however, a weak binding

can still be detected for MAb 155-49. Double mutation didn't affect the binding of MAb 155-49 on imD2VLP, compared to a single

mutation. Only the triple mutation completely abolished the binding of MAb 155-49 on imD2VLP. The antigens used were standardized at a

1175   single concentration with an optical density (OD) of 0.8, which was based on the standard curves generated by antigen-capture ELISA. Data

1176   are shown as means±SEM from three independent experiments. P/N ratio refers to the antibody binding magnitude between designated

1177   VLP-containing (P) and VLP-free culture supernatants (N) by dividing the absorbance of P by that of N.

1178

1179

1180
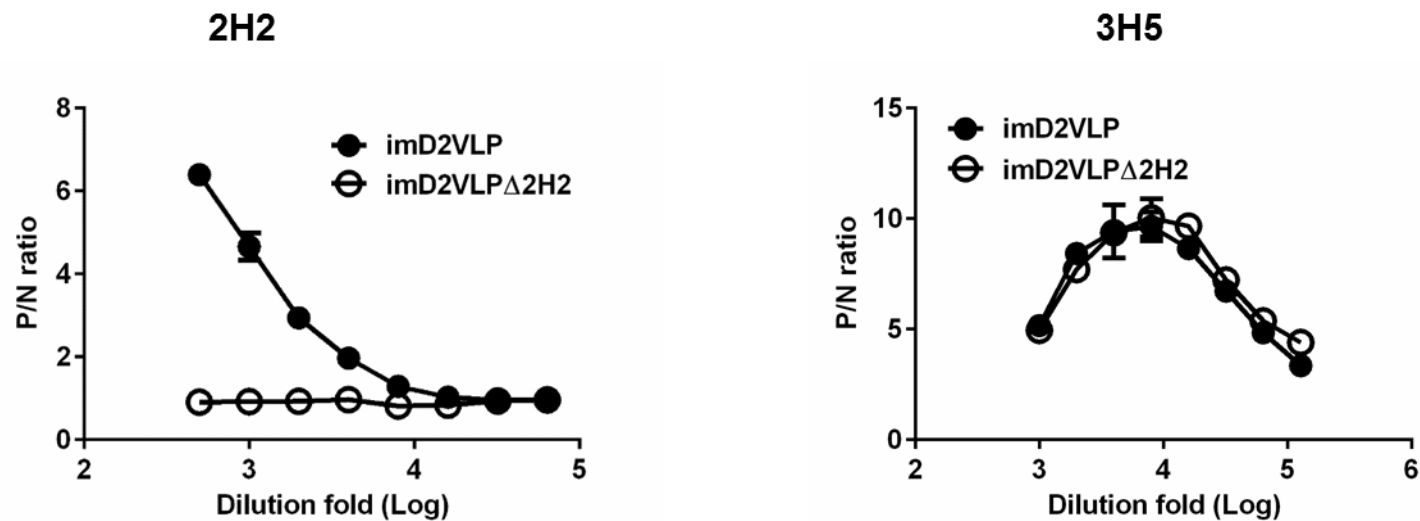
1181

1182 Fig S11. Serial dilutions of imD2VLP and mutant imD2VLP (Δ2H2), containing mutations at the MAb 2H2 binding site (F1A, K21D, K26P), were tested for

1183 binding with MAb 2H2 (left) and control antibody 3H5 (right) by ELISA. P/N ratios refer to the antibody binding magnitude between designated VLP-containing

1184 (P) and VLP-free culture supernatant (N) by dividing the absorbance of P by that of N.

A

B
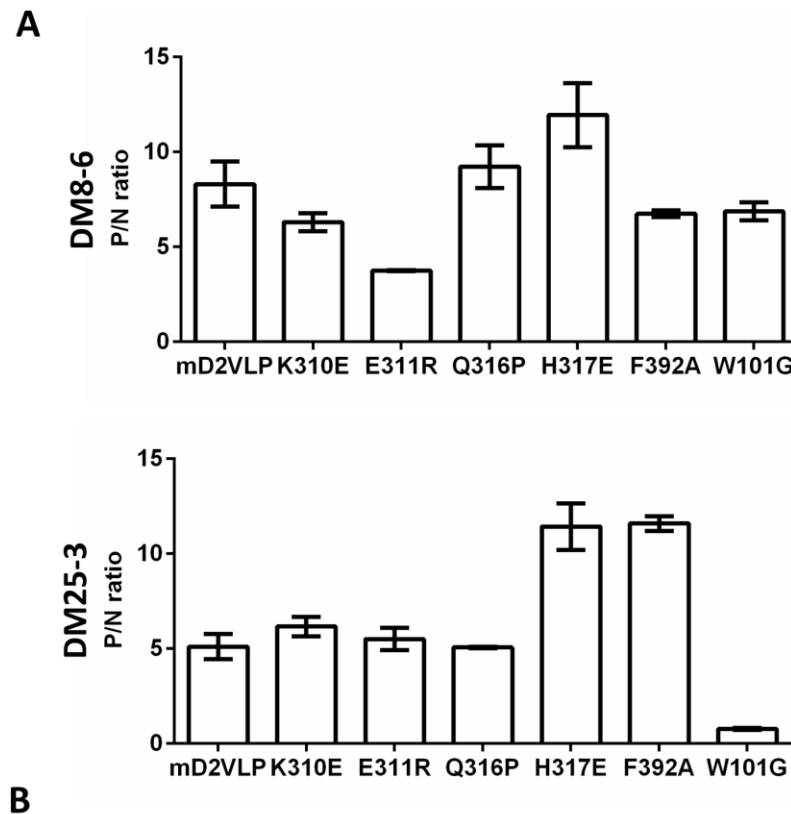
Relative binding (%)	W101G	K310E	E311R
4G2	9±0.7	109.6±5.2	99.4±7.5
4A1B-9	46.3±8.2	84.3±12.2	83.9±4.7
6B3B-3	12.1±0.1	111.9±5.7	82.8±8.2
6B6C-1	40.6±3	127.1±19.8	101±18.9
DM25-3	5.6±0.3	128.6±6.6	98.4±5.9
T5-1	93.4±11.2	12.5±2.1	30.9±2.7
DM8-6	119.5±1.8	89.2±2	41.7±0.5

1185

1186

1187 Figure S12. Identification of the neutralizing epitopes of MAbs DM25-3 and DM8-6. (A) Bar

1188 graph shows the decrease in MAb reactivity in a binding-ELISA for mD2VLPs with

1189 substitutions at the designated residues. Various mD2VLP mutants were expressed in COS-1

1190 cells by electroporation with plasmid DNAs as indicated. Tissue culture media were

1191 harvested 3 days after transfection and clarified for antigen-capture ELISA. Substitutions at

1

1192   N103K, G104Q, K307E, E314R, T315H, P364R and W391G produced plasmids which did

1193   not secrete measurable VLP antigens into the tissue culture medium. Therefore, only mutant

1194   plasmids indicated secreted VLP antigens and were used for epitope mapping by binding

1195   ELISA. (Top) Substitutions of E311E led to a significantly reduced binding activity of

1196   neutralizing MAb DM8-6, compared to mD2VLP. (Bottom) Substitutions of W101G led to a

1197   complete loss of binding by MAb DM25-3. Data shown are a representative experiment of

1198   three independent experiments. (B) To ensure that the antigenic structures were intact, mutant

1199   VLPs including W101G, K310E and E311R were further confirmed by using a panel of

1200   DENV-2 MAbs, including group-cross-reactive antibodies (4G2, 4A1B-9, 6B3B-3, 6B6C-1,

1201   DM25-3) recognizing all four major pathogenic flavivirus serocomplexes; complex cross-

1202   reactive antibodies (T5-1) recognizing all four DENV complex viruses, and type-specific

1203   antibody (DM8-6) recognizing DENV-2 only. The relative binding of MAbs was determined

1204   by dividing the OD_{450} of mD2VLP mutants by that of mD2VLP. The data are presented as means

1205 $\pm$ SEM from three independent experiments with two replicates. The two-tailed Mann-Whitney U test

1206   was   used   to   test   statistical   significance.
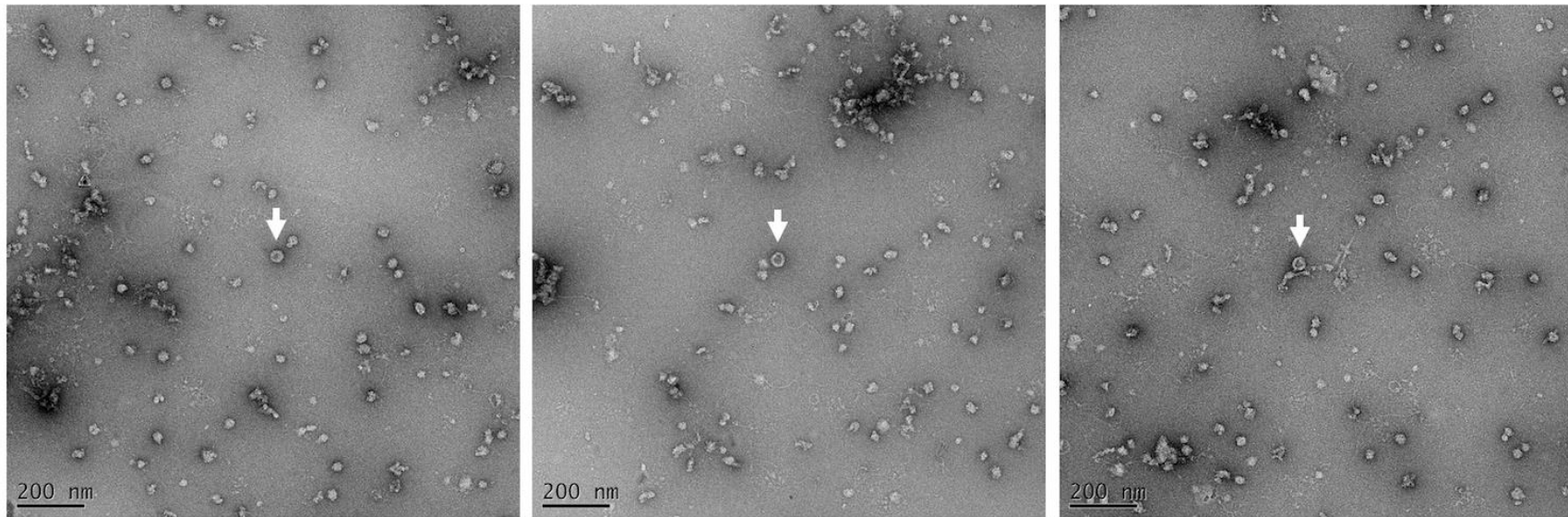
1207

Figure S13. Transmission electron microscope (TEM) examination of negatively stained W101G-mutant mD2VLP. Purified W101G-mutant mD2VLP were adsorbed onto a glow-discharged carbon coated grid (EMS CF-200-Cu) for 1min, and inspected by TEM. The images were taken by a JEM1400 electron transmission microscope at a magnification of 30,000x using a 4k x 4k Gatan 895 CCD camera. The diameters of particles were between 30-32nm as measured by ImageJ software.

1212

1213

1214

```
                                  CDR1                              CDR2
        VH1 : 1    GEPGTSLKISCKTSGYTFTEYTMYWVKQSHGKSLEWIGGINPNNGGTTYNQKFKGKATLT  60

                                  CDR3
        VH2 : 61   VNKSSSIAYMEVRNLTSEDSAVYYCVRYGGYYVFDYWGQGTTLTVSS  107


                                  CDR1                              CDR2
        VL1 : 1    TLWKTQSPASLAVSLGQRATISYRASKSVSTSGYSYMHWNQQKPGQPPRLLIYLVSNLES  60

                                  CDR3
        VL2 : 61   GVPARFSGSGSGTDFTLNIHPVEEEDAATYYCQHIRELTRRRGPSSR      107
```

1215

1216

1217   Figure S14. Amino acid sequences of variable regions of IgH and IgL of antibody DM25-3. The amino acids in the CDR regions are

1218   highlighted in red.

1

1219
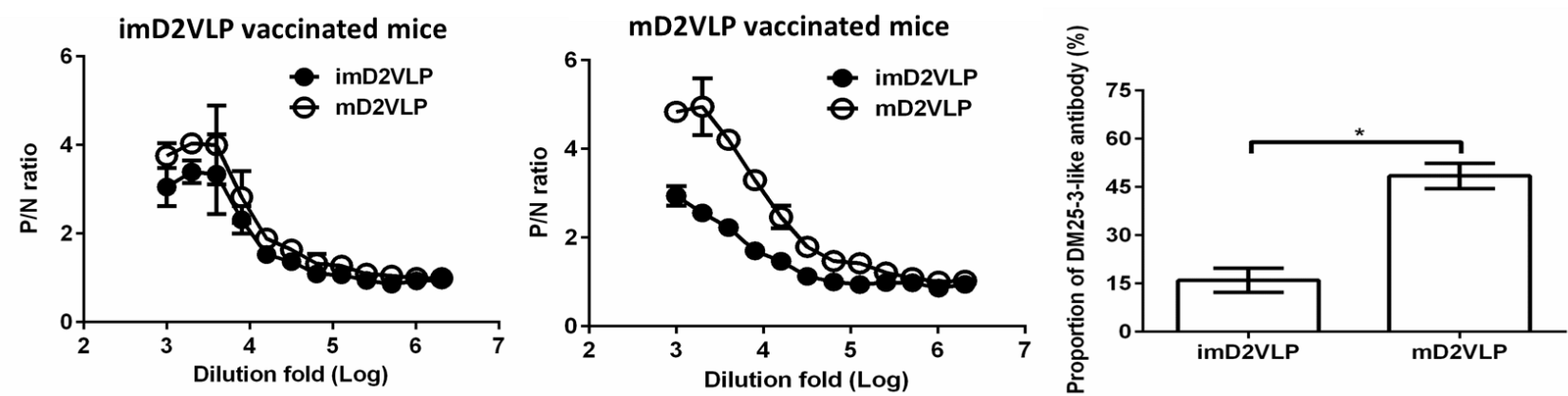
1220

1221   Figure S15. Binding ELISA was performed to test the reactivity of sera from mice immunized with two doses of imD2VLP or mD2VLP

1222   against equal amounts of imD2VLP and mD2VLP antigens. The difference in binding activity was converted to a bar chart at 1:1000-fold

1223   dilutions of mice sera. Proportions of DM 25-3-like antibodies from two different D2VLP immunization groups were calculated based on

1224   the formula $100\text{x}(OD_{450}mD2VLP-OD_{450}imD2VLP)/OD_{450}mD2VLP$. The data are presented as means $\pm$ SEM from three independent experiments

1225   with two replicates. The two-tailed Mann-Whitney U test was used to test statistical significance. *, $P < 0.05$.
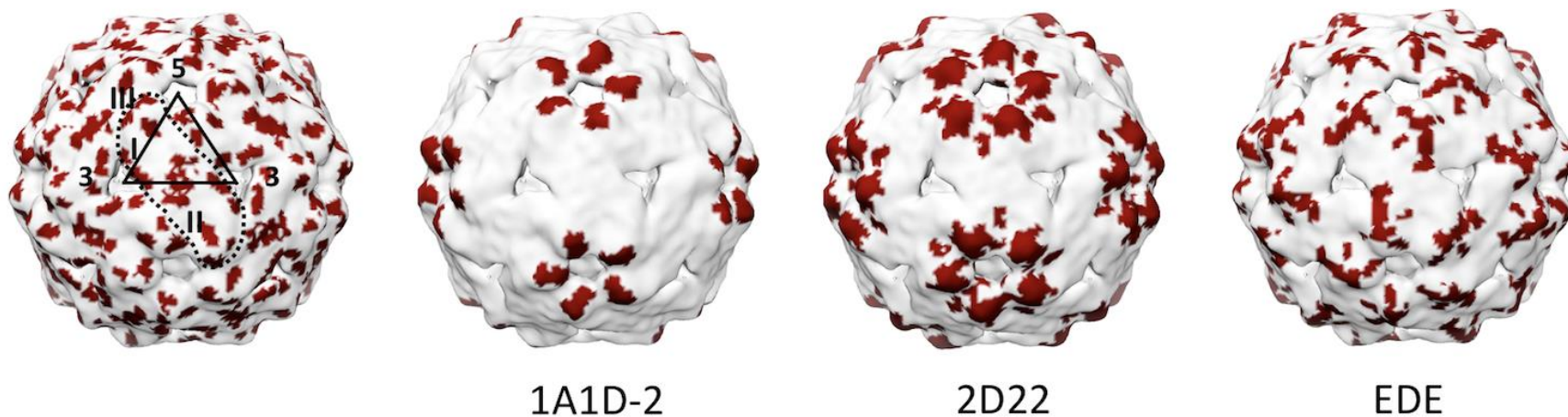
1226

1227

1228

1229

1230   Figure S16. The "neutralization-sensitive hotspot" on mD2VLPs. (Left) The highly exposed residues (Δ%SASA $\geq$ 0.2) which were colored by dark red color are

1231   shown on the surface rendered VLP. The E dimer is outlined by a black dash line, the symmetry and the domains are labeled. The E epitopes interacting with

1232   MAb 1A1D-2 (center left), 2D22 (center right) and EDE (right) are colored in dark red on the surface showing that they were highly exposed on the mD2VLP

1233   surface and were highly overlapping with areas of highly exposed residues in mD2VLP.

1234